



The Early–Middle Palaeozoic Oceanic Events Along the Southern European Margin: The Deli Jovan Ophiolite Massif (NE Serbia) and Palaeo-oceanic Zones of the Great Caucasus

GURAM ZAKARIADZE¹, STEVAN KARAMATA², SERGEI KORIKOVSKY³,
ALEKSEI ARISKIN¹, SHOTA ADAMIA⁴, TAMAR CHKHOTUA⁵,
SERGEI SERGEEV⁶ & NATASHA SOLOV'eva¹

¹ Vernadsky Institute of Geochemistry and Analytical Chemistry, RAS, 119991, Kosigin str. 19, Moscow, Russia
(E-mail: gurzak@geokhi.ru)

² Serbian Academy of Sciences and Arts, 11000 Belgrade, Knez Mihailova 35, SCG
³ IGM RAS, 119017, Staromonetni lane 35, Moscow, Russia

⁴ M. Nodia Institute of Geophysics, 1/1 M. Alexidze str., 0171, Tbilisi, Georgia

⁵ Al. Janelidze Institute of Geology, 1/9 M. Alexidze str., 0193, Tbilisi, Georgia

⁶ Karpinsky Russian Geological Research Institute (VSEGEI), Isotope research Center,
199106 Middle pr. 74, St. Petersburg, Russia

Received 18 November 2010; revised typescripts received 12 May 2011, 18 August 2011,
05 October 2011 & 09 November 2011; accepted 11 December 2011

Abstract: The paper deals with the Middle Palaeozoic oceanic events on the northern margin of the Eastern Mediterranean Hercynides. The Balkan-Carpathian Ophiolite Belt (BCO) and palaeo-oceanic zones of the Great Caucasus, all framing the East European Platform from the south, are correlated. The BCO palaeo-oceanic complex was widely thought to be a Late Precambrian–earliest Cambrian oceanic thrust sheet (563±5 Ma), a part of the South European Palaeo-oceanic Suture. The geochronological studies carried out on gabbroic series of the Deli Jovan Massif (BCO, NE Serbia), showed, however, that they are of much younger (Early Devonian) age: (a) Sm-Nd mineral isochron age of 406±24 Ma, $\epsilon_{Nd_T} = 8.32 \pm 0.39$; $^{87}Sr/^{86}Sr_{init} = 0.702592 \pm 0.000160$; and (b) U-Pb SHRIMP zircon age, 405.0±2.6 Ma. All the studied gabbroic rocks represent high-alumina (19–24.5% Al₂O₃) gabbro-troctolites, originating from shallow level (≤ 2 kb) crystallization of low-K (< 0.3% K₂O) tholeiitic basaltic melts (T= 1190–1350°C). Geochemical and isotopic data for the Balkan-Carpathian ophiolites fit well a MORB-type setting. Thus, the presence of Middle Palaeozoic oceanic events is evident in the BCO, which is important for the evolution of the European Palaeomargin. Data for Lower–Middle Palaeozoic palaeo-oceanic thrust sheets of the Hercynides of the Great Caucasus are also reviewed. The most significant outcrops are located in the Crystalline Core Zone and in the Front Range Zone of the Great Caucasus. These mafic basement complexes in both zones correspond to metamorphosed accretionary wedges consisting, predominantly, of metamorphosed palaeo-oceanic fragments, associated with tonalite-gneisses, plagiogneisses and metasediments. The ophiolite *allochthon* consists of depleted spinel harzburgites, ultrabasic and basic cumulates, sheeted dykes, volcanics and a volcano-sedimentary series. Unlike the BCO almost all the Palaeozoic oceanic series of the Great Caucasus show a clear SSZ imprint. It is assumed that the Middle Palaeozoic oceanic complexes of the Eastern Mediterranean Hercynides apparently correspond to a uniform system of Palaeo-Tethyan marginal basins.

Key Words: Eastern Mediterranean Hercynides, Palaeozoic oceanic events, northern Balkanides, Great Caucasus, Devonian ophiolite

Güney Avrupa Kenarı Boyunca Erken–Orta Paleozoyik Yaşta Okyanusal Olaylar: Deli Jovan Ofiyoliti (Kuzeydoğu Sırbistan) ve Büyük Kafkaslar'da Paleo-okyanus Zonları

Özet: Bu çalışma Doğu Akdeniz Hersinidleri'nin kuzey kenarı boyunca gelişen orta Paleozoyik okyanusal olaylarını konu alır. Bu kapsamda Doğu Avrupa Platformu'nu güneyden saran Balkan-Karpat Ofiyolit Kuşağı ve Kafkaslar'daki paleo-okyanusal zonlar araştırılmıştır. Şimdiye kadar Balkan-Karpat Ofiyolit Kuşağı'nın paleo-okyanusal kompleksinin geç Prekambriyen–en erken Kambriyen (563±5 Ma) yaşında okyanusal kökenli bir bindirme dilimi

oluşturduğu ve Güney Avrupa paleo-okyanusal kenedinin bir kesimini temsil ettiği kabul edilmekteydi. Buna karşın Sırbistan'daki Deli Jovan ofiyoliti gabro serisinde yaptığımız jeokronolojik çalışmalar, bu ofiyolitlerin sanılandan çok daha genç (Erken Devoniyen) olduğunu göstermiştir. Gabrolardan elde edilen Sm-Nd mineral izokron yaşı 406 ± 24 Ma, $\epsilon Nd_1 = 8.32 \pm 0.39$; $^{87}Sr/^{86}Sr_{init} = 0.702592 \pm 0.000160$ 'tır ve yine gabrolardan 405.0 ± 2.6 Ma U-Pb SHRIMP zirkon yaşı bulunmuştur. İncelenen gabro örnekleri, düşük-potasyumlu tholeitik bazaltik magmanın ($T = 1190\text{--}1350^\circ\text{C}$) sıg kesimlerde (≤ 2 kb) kristaleşmesi ile oluşan yüksek alumina içerikli ($\%19\text{--}24.5$ Al_2O_3) gabbro-troktolitleri temsil eder. Balkan-Karpat ofiyolitlerinin jeokimyasal ve izotopik verileri MORB tipi bir tektonik ortama işaret eder. Bu veriler Balkan-Karpat ofiyolitlerinde orta Paleozoyik okyanusal olayların önemini göstermektedir. Büyük Kafkaslar Hersiniyen dağ kuşağındaki erken–orta Paleozoyik yaştaki paleo-okyanusal bindirme dilimleri de bu çalışmada irdelenmiştir. Bu dilimlerin en önemli mostraları Büyük Kafkaslar'ın Kristalen Çekirdek ve Ön Silsile zonlarında yer alır. Her iki zondaki mafik temel kompleksler metamorfizma geçirmiş dalma-batma komplekslerini temsil eder ve tonalit-gnays, plajiyog-nnays and metasedimanter kayalar ile birlikte bulunan paleo-okyanusal parçalardan oluşur. Ofiyolit allokonları tüketilmiş spinel-harzburgitlerden, ultrabazik ve bazik kümülatlardan, levha dayklarından, volkanik ve volkanosedimenter serilerden yapılmıştır. Balkan-Karpat ofiyolitlerinden farklı olarak Büyük Kafkaslar'daki hemen hemen tüm Paleozoyik okyanusal seriler dalma-batma zonu üstünün jeokimyasal özelliklerini taşır. Doğu Akdeniz bölgesi Hersinidleri'nin orta Paleozoyik okyanusal kompleksleri Paleo-Tetis'in kenar deniz özelliklerini göstermektedir.

Anahtar Sözcükler: Doğu Akdeniz Hersinidleri, Paleozoyik okyanusal olayları, kuzey Balkanidler, Büyük Kafkaslar, Devoniyen ofiyoliti

Introduction

Numerous Cadomian blocks of peri-Gondwanan affinity are recognized in the crystalline basement of the European Hercynides, which is one of the fundamental features of the Hercynian belt (Matte 1991; Pharaoh 1999; Crowley *et al.* 2000; von Raumer *et al.* 2002, 2003; Keppie *et al.* 2003 and references therein). The detachment of blocks (terranes) from the northern Gondwana margin started during the Middle to latest Ordovician, when the Palaeo-Tethys basin started to open. Thus, identification and study of the peri-Gondwanan terranes included in the vast Hercynian belt reveals the evolution of the active Gondwana margin in the Neoproterozoic and earliest Palaeozoic, as well as the evolution of the Palaeo-Tethys Ocean. In this respect Neoproterozoic–Cambrian terranes and associated younger (pre-Upper Carboniferous) ensimatic complexes are of special interest.

In this paper we describe a case exemplifying a Lower Palaeozoic ophiolite belt (Thracian Palaeo-oceanic Suture) at the junction of the South Carpathian and Northern Balkan terranes of southeastern Europe. The major features of this suture were previously described in a series of publications (Terzić-Perković 1960; Haydoutov 1989, 1991; Haydoutov *et al.* 1993, 1996–1997; Karamata & Krstić 1996; Karamata *et al.* 1996–1997; Haydoutov & Yanev 1997; Savov *et al.* 2001, etc). It was shown

to include well-preserved N-MORB-type ophiolite successions (Haydoutov 1991), immature island arc-type sequences associated with *ophiolitoclastic olistostromes*. These are overlain by Lower–Middle Palaeozoic terrigenous sequences. The oceanic and island arc sequences of the suture were dated as Neoproterozoic–Cambrian and the whole association was interpreted as a peri-Gondwanan terrane (Haydoutov 1991; Haydoutov & Yanev 1997; Savov *et al.* 2001). Unlike these widely accepted results, our studies of gabbroic rocks from the Deli Jovan Massif of the Balkan-Carpathian ophiolites (BCO, Savov *et al.* 2001) have established a much younger (Devonian) age for this oceanic sequence.

Description of these results and their possible consequences is the primary goal of this paper. Also, in relating the Middle Palaeozoic magmatic events to processes related to the evolution of the European palaeomargins, we have attempted to correlate the major features of the Thracian Suture with the Middle Palaeozoic Palaeo-oceanic suture zones of the Great Caucasus, which are in a similar geological position in the Eastern Mediterranean Hercynides (Figure 1). Data on the Great Caucasus are presented as a brief review, based on representative publications and unpublished materials of authors (Shavishvili 1983; Adamia 1989; Shengelia *et al.* 1991; Somin 1991, 2009; Perchuk & Philippot 1997; Adamia *et al.* 2004, 2010; etc).

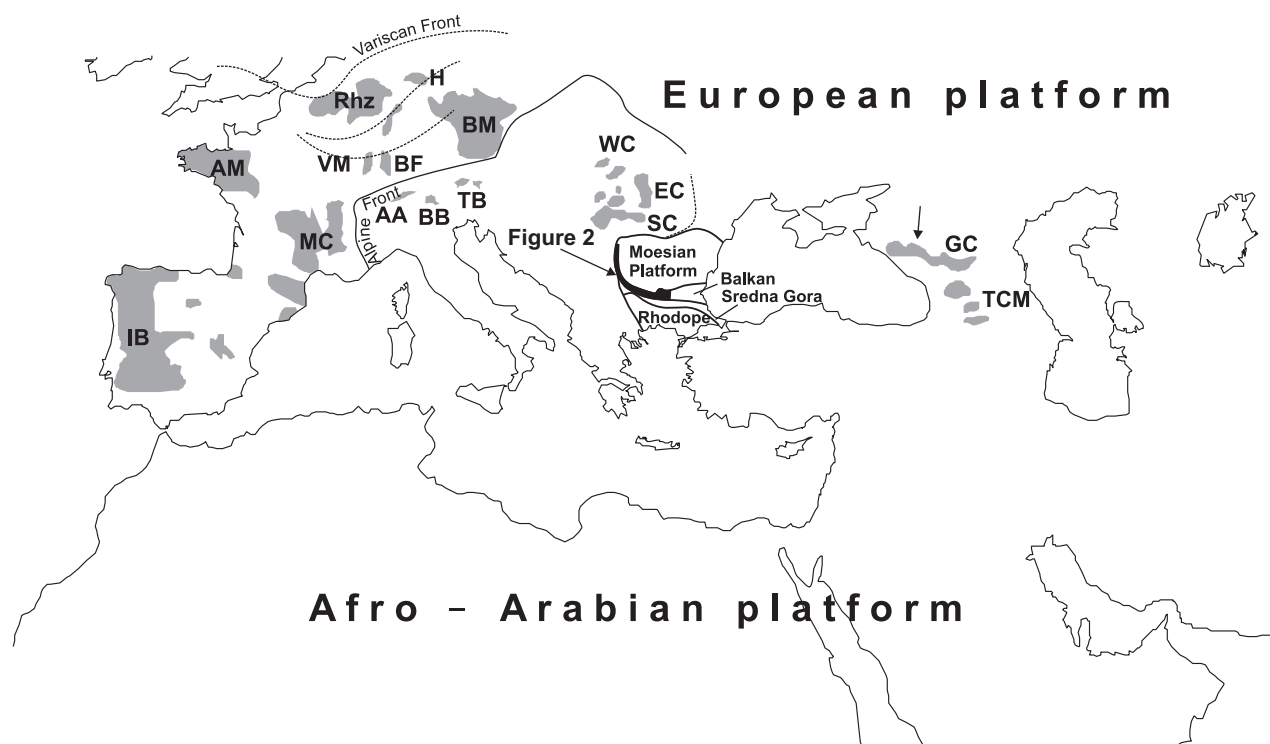


Figure 1. Simplified geological map of the European Variscan Massifs. IB– Iberian Massif, AM– Armorica Massif, MC– Massif Central, VM– Vosges Massif, BF– Black Forest Massif, AA– Aar Batholith, BB– Bernina Batholith, TB– Tauern Batholith, BM– Bohemian Massif, H– Harz Massif, WC, EC, SC– Western, Eastern and Southern Carpathians; GC– Great Caucasus; TCM– Transcaucasian Massif (after Carrigan *et al.* 2005, modified).

Geological Setting and Internal Stratigraphy of the BCO

The Lower Palaeozoic Ophiolite belt is exposed in Eastern Serbia, extending north across the River Danube into southwestern Romania and southeastwards to westernmost Bulgaria. This belt is more than 200 km long in Serbia, with about 25 km in Romania to the north, and about 25 km in Bulgaria to the southeast (Figures 1 & 2).

Along the belt, the major palaeo-oceanic blocks are represented by separate massifs: Tcherni Vrah, and smaller Pilatovetz, Stara Reka, Kopilovtzi (Stara Planina mountains, Bulgaria); Tisovita, Donji Milanovac, Zaglavak and Deli Jovan (Serbia; Deli Jovan mountains); and South Banat (Romania SE Carpathians), comprising in total a complete ophiolite sequence (Haydoutov 1991; Savov *et al.* 2001). It is assumed that these massifs are the remnants of a single ophiolite thrust sheet and hence have a similar origin and evolutionary path. Ophiolite allochthons

were emplaced along the Thracian Palaeo-oceanic Suture at the boundary of the Moesian and Thracian Precambrian continental blocks and are unconformably overlain by a *Cambrian* volcano-sedimentary arc-related sequence (Berkovitza Group-Stara Planina Bulgaria; and Vlasinski Complex of the Serbo-Macedonian massif, Serbia). These are overlain by a Lower–Middle Palaeozoic unmetamorphosed sedimentary cover (Figure 3; Haydoutov & Yanev 1997; Haydoutov *et al.* 1997; Savov *et al.* 2001). The whole sequence of Thracian suture rocks, including Lower Palaeozoic and Variscan granitic intrusions, are now incorporated in the Alpine Upper Danubian nappe system of the Carpatho-Balkanides and thrust over the Precambrian continental basement of the Moesian Platform (terrane), or the Poreč terrane (Stara Planina – Poreč unit: Karamata & Krstić 1996; Karamata *et al.* 1996).

Mantle Restites (ultramafic tectonites) of the palaeo-oceanic sequence are exposed only in

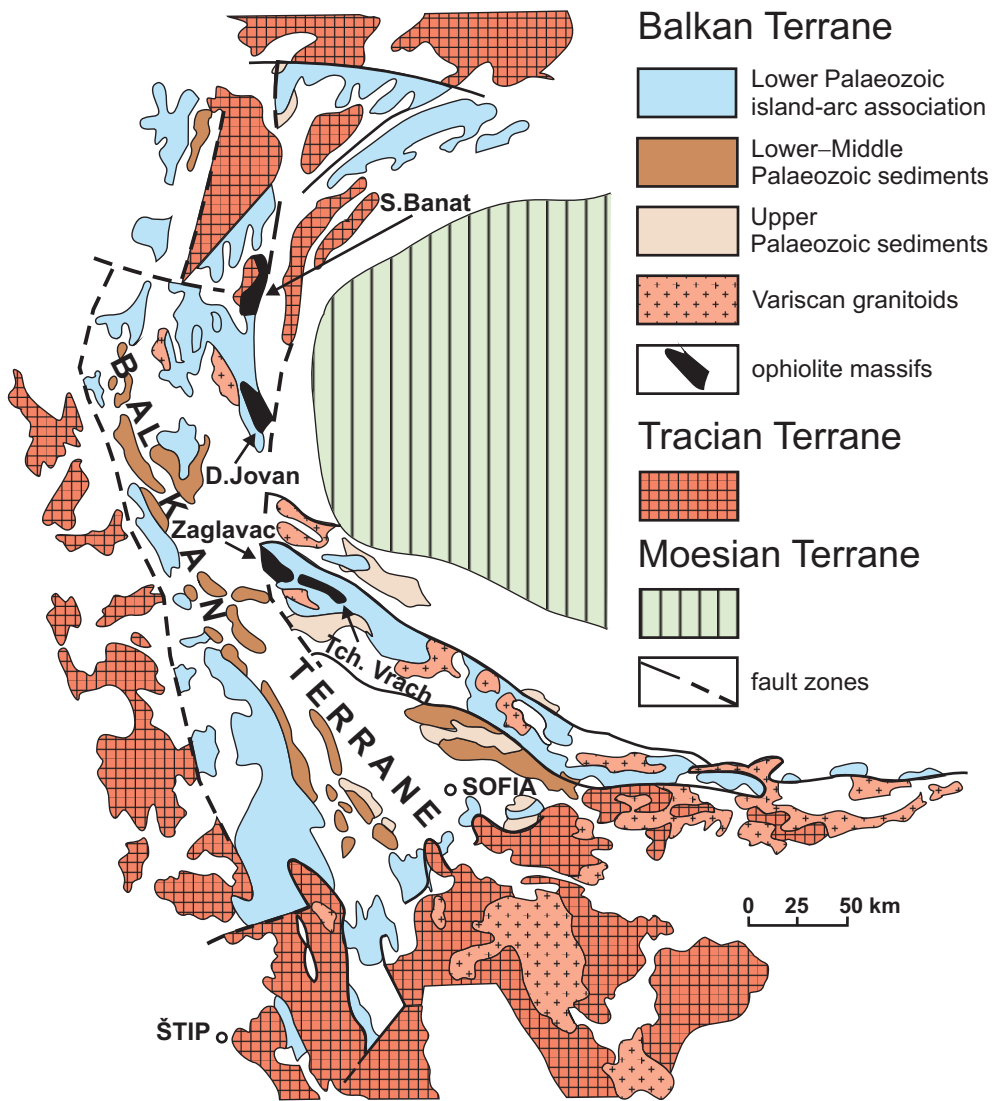


Figure 2. Geological sketch of the Balkan Terrane, area of distribution of Balkan-Carpathian ophiolites (BCO, after Haydoutov & Yanev 1997; simplified)

the South Banat Massif and consist of sheared harzburgites with lenses of dunites (Măruntiu 1984). The internal stratigraphy and composition of the Deli Jovan, Zaglavac and Tcherni Vrach massifs are in general quite similar (Terzić-Perković 1960; Haydoutov & Yanev 1997; Haydoutov *et al.* 1997; Savov *et al.* 2001). The most representative data on the magmatic part of the palaeo-oceanic sequence are known from Cherni Vrach and to a lesser degree from the Deli Jovan Massif. The brief description below is based on previous data (Haydoutov 1989,

1991; Haydoutov *et al.* 1993; Haydoutov & Yanev 1997; Savov *et al.* 2001; etc). Much of the magmatic series consist of ultramafic and mafic cumulates and gabbros, subordinate sheeted dykes and basaltic lavas with minor lenses of argillites. The cumulate section of the Tcherni Vrach Massif is composed of ultramafic cumulates and gabbros and has a total thickness of 2.5 km. The lower boundary of this sequence is tectonic, while the upper boundary grades through isotropic gabbro into sheeted dykes. The lower cumulate sequence includes relatively

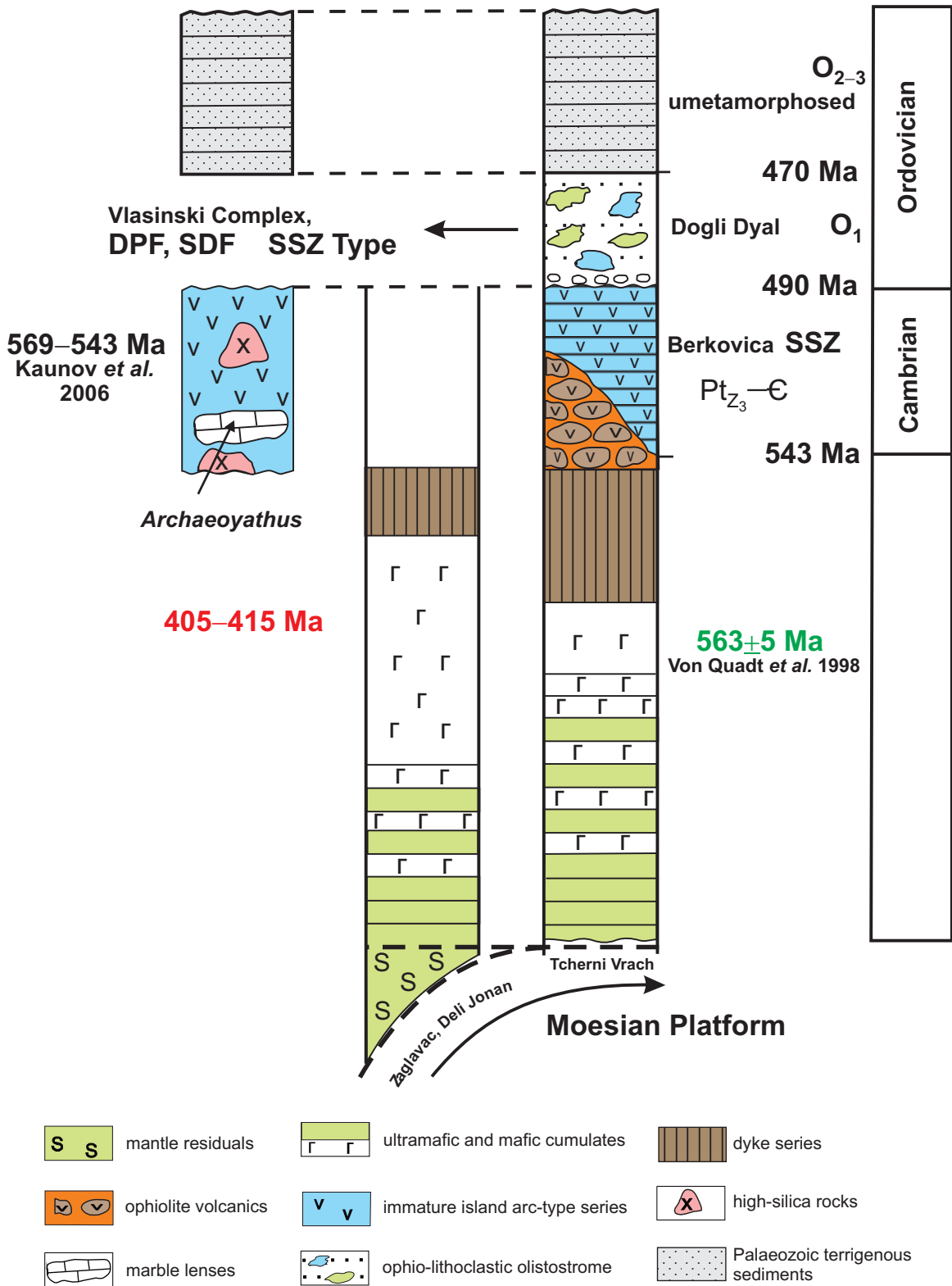


Figure 3. Geological columns of the Balkan-Carpathian ophiolites (compiled from Savov et al. 2001). DPF– diabase-phyllitoid formation; SDF– Struma-diorite formation; SSZ– supra-subduction zone.

thin (0.15–6 m) alternating layers of gabbros and ultramafic cumulates (dunites, wehrlites, plagioclase wehrlites, troctolites, olivine gabbros, pyroxenites and anorthosites). The upper cumulate sequence lacks ultramafic rocks and is dominated by gabbros. The gabbros alternate with lenses of anorthosite, pyroxenite and pegmatoid gabbro, giving the unit a layered appearance.

The sheeted dyke unit has a total thickness of ~1 km. Its upper boundary is gradational with dykes cross-cutting basalt lava flows. Dykes, 5–7 m thick, intrude each other and many have chilled margins. All have similar strikes and dips.

The extrusive section at Tcherni Vrah forms a 20-km-long mappable unit up to 700 m thick. It consists of alternating pillow lavas, lava tubes and massive basalt flows overlain by hyaloclastites, lava breccias and sediments. The Deli Jovan Massif of northeastern Serbia also consists of ultrabasic and basic cumulates, sheeted dykes and volcanics. The contacts of the massif with all surrounding formations are tectonic (Figure 4).

Based on the relative thicknesses of the mafic and ultramafic cumulates Haydoutov (1991) divided the cumulate sequences of the massif into eastern and western parts. The eastern part includes layers of dunites, troctolites, olivine gabbros, wehrlites and anorthosites, alternating with fine-grained gabbros. The western part of cumulates is composed of locally pegmatoid coarse-grained and undeformed gabbros with little or no ultramafic cumulates. As a whole, homogeneous, isotropic gabbro is the dominant rock type of the Deli Jovan Massif. Important features of the BCO palaeo-oceanic sequence are the gradational boundaries between major ophiolite magmatic units and clear similarities between the strikes of the sheeted dykes and the elongation of preserved lava tubes in the pillow lavas that allows little relative motion among the units of the ophiolite complex to be assumed since their formation as igneous sequences (Savov *et al.* 2001).

Areas of Sampling and Petrographic Features of Studied Rocks of the Deli Jovan Massif of NE Serbia

We investigated six representative samples from different parts of the Deli Jovan Massif, five gabbros and one diabase dyke. All the gabbroic samples are

from the level of homogeneous gabbros, between the cumulate ultramafics and the roots of the diabase dykes. This horizon corresponds to the thickest part of the gabbros, where they are mainly isotropic, coarse, and only locally very coarse-grained. Sometimes layers of olivine-bearing cumulates to ultramafic varieties occur in this levels. Sampling localities (1–4) are indicated on Figure 4: (1) Gabbro samples DJ-1-03, DU-2-03 ($x=4894,300$; $y=7601,500$) were collected from the eastern part of the massif, 3–4 km west of the village of Sikole. (2) Gabbro sample DJ-4-98 ($x=4894,300$; $y=7602,500$) is from northern slopes of Perina Cuka, north of the village of Glogovica, in the southern part of the Deli Jovan Massif. (3) Diabase dike DJ-1-98 ($x=4893,200$; $y=7602,400$) is from the western side of the village of Mala Jsikova; in the southern part of the Deli Jovan Massif. (4) Gabbro samples DJ-5-98 ($x=4903,100$; $y=7592,800$), and DJ-6-98 ($x=4903,100$; $y=7592,850$) are relatively olivine rich. Samples are from the Vamna stream, on the western slopes of Mali Goli Vrh Crnajka.

Gabbroic series of the Deli Jovan Massif are generally fresh and are partially affected by low-temperature metamorphic changes. The studied samples include both varieties. Fresh gabbros are represented by samples DJ-1b-03, DJ-1c-03 DJ-5-98 and DJ-6-98 (Figure 5a, b).

Sample DJ-1b-c; Olivine-Plagioclase-Clinopyroxene High-Al Gabbro is composed predominantly of prismatic calcic plagioclase adcumulates and subordinate anhedral crystals of olivine and clinopyroxene. Relations of olivine and clinopyroxene are of two kinds. They either form separate large crystals, usually as aggregates, or thin clinopyroxene rims of olivine. Olivine-clinopyroxene segregations are often associated with grains of Fe-Ti oxides.

Sample DJ-5-98; Fresh High-Al Troctolitic Gabbro is composed predominantly of large unzoned adcumulate euhedral crystals of calcic plagioclase and by separate irregular anhedral crystals of olivine and clinopyroxene. The latter either forms irregular separate grains or thin rims around olivine at contacts zones with plagioclase. Minor Fe-Ti oxides are associated with Mg-Fe silicates.

Sample DJ-6-98; Olivine-Clinopyroxene-Plagioclase High-Al Gabbro is substantially identical

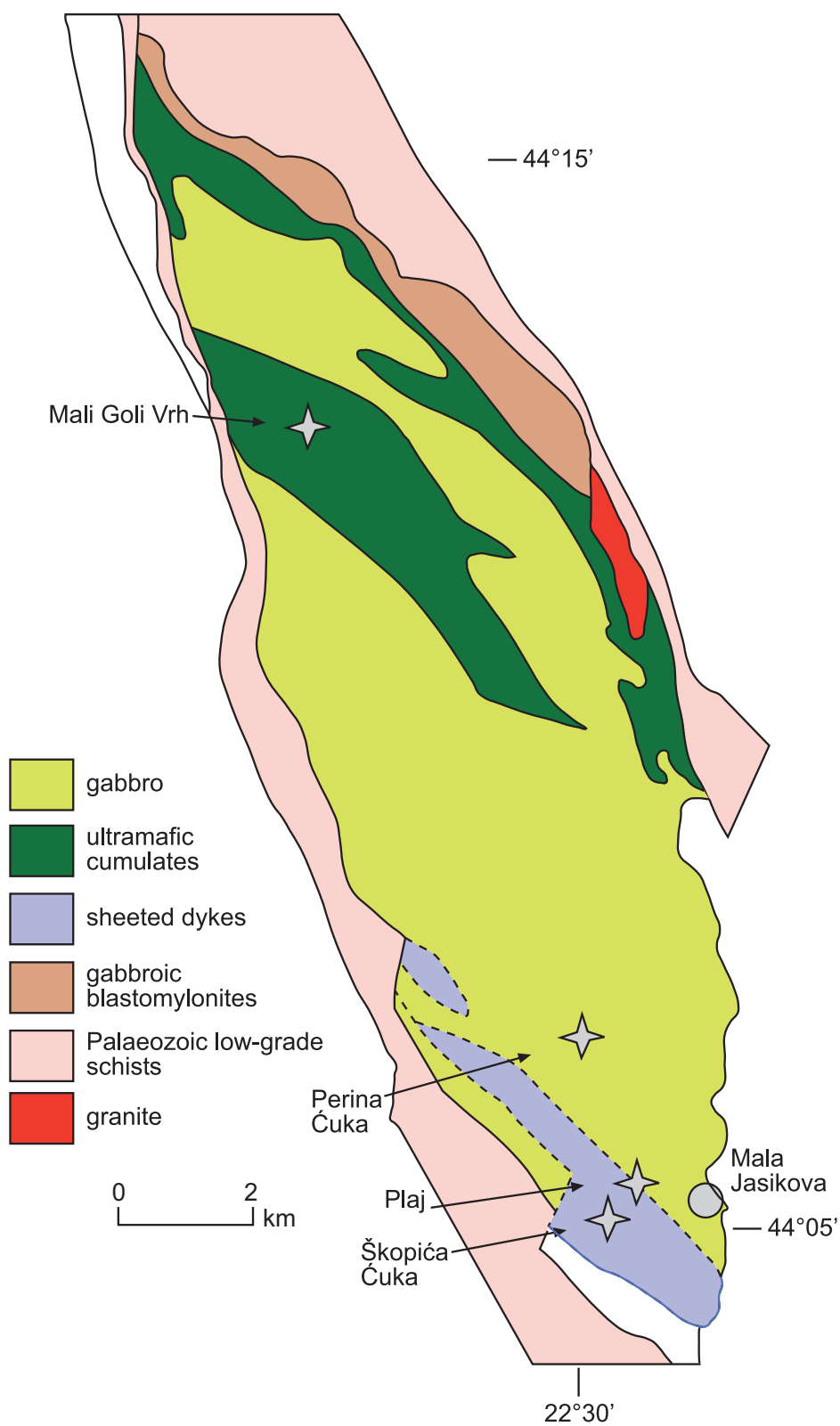


Figure 4. The Deli Jovan gabbro massif. Map compiled and simplified by S. Karamata. Asterisks– location of villages; white squares– sampling locations.

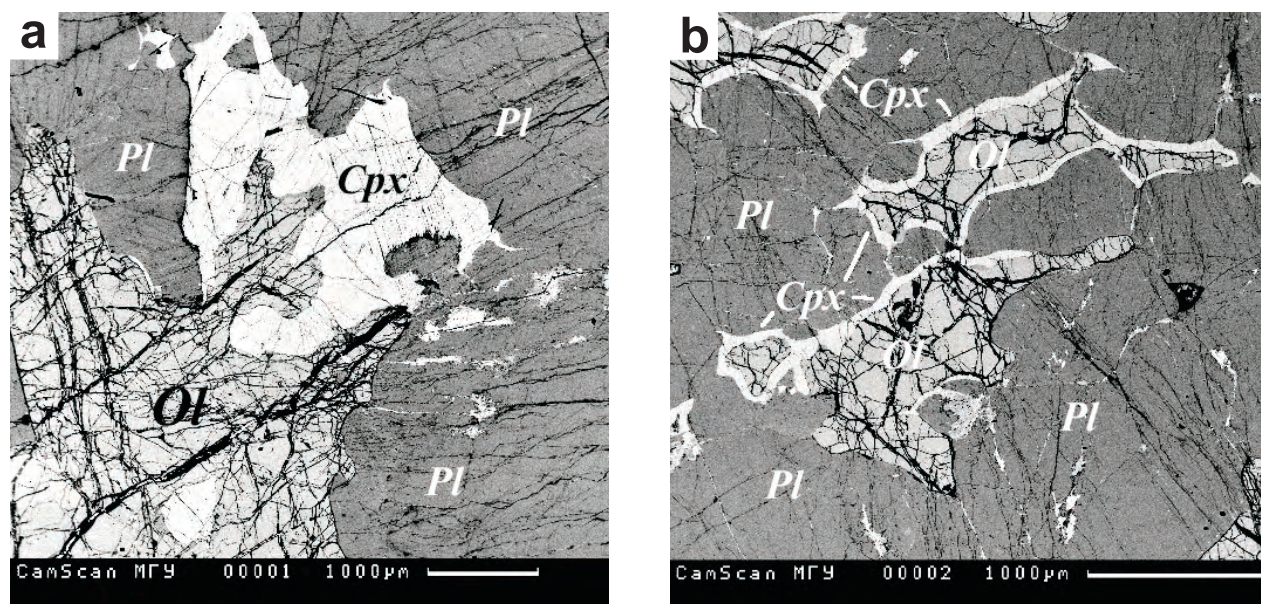


Figure 5. Relationships of anhedral crystals of olivine with clinopyroxene rims and prismatic plagioclase adcumulates in the Deli Jovan gabbros.

to the previous sample. Euhedral prismatic unzoned crystals of calcic plagioclase are the dominant phase. Olivine and clinopyroxene occur as separate irregular anhedral grains. In places clinopyroxene forms thin rims around olivine along contact zones of the latter with plagioclase. Minor Fe-Ti oxides are associated with Mg-Fe silicates.

Sample DJ-1-98; Marginal Part of Dyke – Plagioclase-Clinopyroxene Phyric Subvolcanic Microgabbro (Gabbro-Diabase) Phenocrysts (~ 30% of the rock) are represented by fresh prismatic crystals of calcic plagioclase. Well-developed fresh clinopyroxene single phenocrysts are rarely seen. The groundmass is holocrystalline (diabasic) and composed of idiomorphic plagioclase, xenomorphic clinopyroxene and rare segregations of Fe-Ti oxides. Clinopyroxene is irregularly replaced by the actinolite-epidote-chlorite association.

Altered gabbros correspond to samples *DU-2-03 and DJ-4-98*. Alteration is expressed by formation of actinolite-epidote-chlorite rims or complete pseudomorphism of clinopyroxene and various veinlets filled by epidote and chlorite. Extensive replacement of clinopyroxene by apparently secondary amphibole is also displayed. Everywhere in spaces between plagioclase crystals an actinolite-

chlorite-epidote-Fe-Ti oxide association is developed. The main features of metamorphic changes are considered in more detail in the section on results.

Analytical Procedures

The mineral chemistry was examined on polished thin sections by CAMECA CAMEBAX and CAMECA SX-100 electron microprobes at the Vernadsky Institute of Geochemistry and Analytical Chemistry RAS, Moscow, using an accelerating voltage of 15 kV and beams with a current of 35 nA. Natural and synthetic minerals were used as standards. Major and trace-element analyses were performed for a basic series by XRF by Roshchina I.A. & Romashova T.V. using a Phillips PW-1600 instrument in the Vernadsky Institute. The initial sample weight for the most analyzed rocks was at least 200 g. The calibration was performed using international and domestic rock standards, together with internal standards. The attested values of international standards were adopted (Govindaraju 1994).

Inductively-coupled plasma mass spectrometry (ICP-MS) analyses were carried out in the Institute of Mineralogy, Geochemistry and Crystal Chemistry of Rare Elements of the Geological Survey of Russia

(Moscow). Mass-spectrometric analyses were performed on an Elan 6100 DRC [ELAN 6100 DRC, Software Kit, May 2000, PerkinElmer SCIEX instrument] in a standard mode. The calibration of the instrument sensitivity according to the entire scale of masses was accomplished with the aid of standard solutions, which include all the analyzed elements in probes. The instrument analyses of probes alternated with analyses of the external standard basalt BCR-2 (US Geological Survey). Detection Limits (DL) of elements were from 1–5 (ppb) for the heavy and middle elements (uranium, thorium, REE, etc) to 20–50 ppb for light elements (beryllium etc.). Analytical accuracy was 3–10% (rel.) for the concentrations of elements above 20–30 of DL by Analyst D.Z. Zhuravlev.

U-Pb dating of zircons was carried out on a secondary high resolution ion microprobe (SHRIMP-II) in the Karpinsky Russian Geological Research Institute, Isotope Research Centre (VSEGEI), Saint-Petersburg, Russia. Hand-packed grains of zircons were implanted in epoxy resin together with grains of zircon standard TEMORA. The zircon grains then were co-polished and ground to approximately half their thickness. For choice of sites (points) for dating on the grain surfaces optical (transmitted and reflected light) and cathode-luminescent images by scanning electronic microscope were used, reflecting the internal structure and zoning of zircons. U-Pb ratio measurements on the SHRIMP-II mass-spectrometer were carried out by a technique described by Williams (1998). Intensity of the primary beam of the molecular negatively charged ions of oxygen made 5 nA; the diameter of the spot (crater) was 25 microns.

The geochronological data was processed by SQUID (Ludwig 2000). U-Pb ratios were normalized on the value 0.0668, attributed to standard zircon TEMORA that corresponds to age of this zircon 416.75 million years (Black *et al.* 2003). Errors of individual analyses (ratios and age) are given at the level of one sigma, errors of calculated concordant ages and crossings with concordia are shown at the level of two sigma. Construction of graphs with concordia (Wetherill 1956) was carried out with use of the ISOPLOT/EX program (Ludwig 1999).

Nd and Sr Isotope analyses were carried out by S. Karpenko in the Vernadsky Institute of Geochemistry RAS, Moscow. The sample was spiked with isotope tracers $^{87}\text{Rb}+^{84}\text{Sr}$ and $^{149}\text{Sm}+^{150}\text{Nd}$ and then digested by a mixture of concentrated HF and HNO_3 within 1–3 days at temperatures between 80–90°C. Separation of Rb, Sr, Sm and Nd was made by the usual techniques (Richard *et al.* 1976).

Mass-spectrometric measurements of the isotopic composition of strontium and neodymium, as well as determination of rubidium, strontium, samarium and neodymium contents by means of isotopic dilution was carried out on TRITON TI mass-spectrometers working in static mode with the use of a two-tape (Re+Re) source of ions. The accuracy of measurements was constantly checked by measurement of isotope standards SRM 987 and La Jolla and standard BCR-1. In all cases errors of determination of isotopic composition of Sr and Nd were much less than 0.005%, and errors of determination of the ratios $^{147}\text{Sm}/^{144}\text{Nd}$ and $^{87}\text{Rb}/^{86}\text{Sr}$ were less than 0.2%. The specified values of errors of measurements have been used further in the calculation of the isochron age of the investigated rocks (Ludwig 1999). Intra-laboratory contamination of blanks in all cases appeared negligible and was not considered during the interpretation.

Results

Petrological Identification of Protoliths of the Studied Gabbroic Series

The total thickness of the BCO cumulate sequence and related gabbros has been estimated as 2.5 km, demonstrating wide variations in modal proportions of three main constituent minerals – olivine, plagioclase, and clinopyroxene. In places, subordinate orthopyroxene and primary amphibole are also mentioned (Savov *et al.* 2001). All gabbroic samples were taken from the level of ‘the homogeneous gabbros’ located between the cumulate sequence and the roots of the diabase dykes. This horizon corresponds to the thickest portion of gabbros of this type. The fresh gabbros (samples DJ-1b-03, DJ-1c-03, DJ-6-98) contain the assemblage $\text{Ol}_{83-84}+\text{Cpx}_{84-87}+\text{Pl}_{77-92}$ plus accessories, Fe-Ti oxide, titanite, apatite, ilmenite. The Mg# of olivine and Ca-rich

clinopyroxene (augite) is almost constant, whereas the composition of plagioclase ranges from bytownite to anorthite (two groups of Pl_{82-77} and Pl_{90-92}). In total, calcic plagioclase is a much more abundant phase than mafic minerals in all the investigated samples. Figure 5 demonstrate adcumulate-like relations between anhedral olivine crystals, clinopyroxene rims, and the plagioclase prisms. Representative compositions of olivine, clinopyroxene and plagioclase are given in Tables 1 to 3.

Major and trace element compositions for six representative rocks of the gabbroic sequence are given in Tables 4 & 5 and Figures 6–8, where the data from the Tcherni Vrah Massif are shown for comparison (Savov *et al.* 2001). Our gabbroic samples correspond to low-K (<0.1% K_2O), slightly silica-undersaturated,

olivine-diopside-hypersthene normative tholeiites. They might be classified as high-magnesia ($Mg\#=0.74\pm0.07$) and low-Ti ($TiO_2=0.16\pm0.13\%$) basaltic rocks, which are extremely enriched in alumina ($Al_2O_3=22.36\pm2.01\%$). The obvious gap in contents of incompatible elements, such as Ti, P, and REE, between the cumulate plutonic and volcanic samples (Figures 7c & 8) is a common feature for many oceanic (ophiolitic) type successions (Natland & Dick 2001 and references therein). The high-alumina compositions are characteristic of almost all levels of the BCO complex, especially in ultramafic and mafic cumulate units. Co-variation in Al vs Ca, REE patterns, and positive Eu and Sr anomalies indicate the importance of plagioclase crystallization/accumulation in the BCO magma chambers. To

Table 1. Microprobe results for olivine from the Deli Jovan gabbros.

Sample	DJ-6-GAB2	DJ-6-GAB3	DJ-6-GAB4	DJ-6-98-1	DJ-6-98-2	DJ-6-98-3	DJ-1c-1	DJ-1c-2	DJ-1c-3	DJ-1c-4
SiO ₂	39.3	39.22	39.29	39.32	39.63	39.26	39.54	39.55	39.38	39.38
TiO ₂	n.d.	n.d.	n.d.	n.d.	0.01	n.d.	n.d.	n.d.	n.d.	n.d.
Al ₂ O ₃	0.01	0.02	n.d.	n.d.	n.d.	n.d.	n.d.	n.d.	n.d.	n.d.
Cr ₂ O ₃	0.03	0.01	n.d.	0.03	n.d.	0.04	0.03	0.16	0.01	0.01
FeO	17	16.78	16.52	16.73	16.51	16.08	15.94	15.47	15.48	15.48
MnO	0.16	0.29	0.21	0.19	0.29	0.32	0.26	0.23	0.27	0.27
MgO	44.36	44.51	43.88	43.71	43.83	43.6	44.18	44.56	44.49	44.49
CaO	n.d.	n.d.	0.02	0.02	0.06	0.01	0.03	0.03	0.03	0.03
Na ₂ O	n.d.	n.d.	n.d.	n.d.	n.d.	n.d.	n.d.	n.d.	n.d.	n.d.
K ₂ O	n.d.	n.d.	n.d.	n.d.	n.d.	n.d.	n.d.	n.d.	n.d.	n.d.
Total	100.86	100.83	99.92	100.00	100.33	99.31	99.98	100.00	99.66	99.66
Si	0.98	0.98	0.99	0.99	1.00	1.00	1.00	1.00	0.99	0.99
Ti	n.d.	n.d.	n.d.	n.d.	n.d.	n.d.	n.d.	n.d.	n.d.	n.d.
Al	n.d.	n.d.	n.d.	n.d.	n.d.	n.d.	n.d.	n.d.	n.d.	n.d.
Cr	n.d.	n.d.	n.d.	n.d.	n.d.	n.d.	n.d.	n.d.	n.d.	n.d.
Fe ³⁺	0.03	0.04	0.01	0.01	n.d.	n.d.	n.d.	0.01	0.01	0.01
Fe ²⁺	0.33	0.32	0.34	0.34	0.35	0.34	0.33	0.32	0.31	0.31
Mn	0.00	0.01	0.00	0.00	0.01	0.01	0.01	0.00	0.01	0.01
Mg	1.66	1.66	1.65	1.65	1.65	1.65	1.66	1.67	1.67	1.67
Ca	n.d.	n.d.	n.d.	n.d.	n.d.	n.d.	n.d.	n.d.	n.d.	n.d.
Na	n.d.	n.d.	n.d.	n.d.	n.d.	n.d.	n.d.	n.d.	n.d.	n.d.
K	n.d.	n.d.	n.d.	n.d.	n.d.	n.d.	n.d.	n.d.	n.d.	n.d.
X(Fo)	0.84	0.84	0.83	0.83	0.83	0.83	0.83	0.84	0.84	0.84
X(Fa)	0.16	0.16	0.17	0.17	0.17	0.17	0.17	0.16	0.16	0.16

Fo– forsterite; Fa– fayalite.

Table 2. Microprobe results for clinopyroxene from the Deli Jovan gabbros.

Sample	DJ-6-GAB1	DJ-6-GAB2	DJ-6-98-1	DJ-6-98-2	DJ-6-98-3	DJ-6-98-4	DJ-6-98-5	DJ-6-98-6	DJ-1c-1	DJ-1c-2	DJ-1c-3
SiO ₂	51.9	51.3	51.96	51.81	52.12	51.28	51.86	51.75	51.14	50.75	51.81
TiO ₂	0.39	0.55	0.47	0.4	0.46	0.77	0.67	0.63	1.14	1.12	0.63
Al ₂ O ₃	3.09	2.82	4.06	3.78	3.41	3.72	3.72	3.78	3.75	3.74	3.54
Cr ₂ O ₃	1.02	1.02	0.94	1.05	0.87	0.87	0.91	0.89	0.81	1.35	0.8
FeO	6.08	4.62	4.71	5.03	4.05	4.35	4.35	4.48	4.26	5.41	4.55
MnO	0.13	0.14	0.17	0.19	0.11	0.13	0.11	0.12	0.16	0.19	0.2
MgO	17.76	16.06	16.9	16.82	15.9	15.5	15.84	15.72	15.88	16.7	16.96
CaO	20.17	23.2	20.63	20.49	23.08	22.67	22.49	22.92	22.7	20.4	21.41
Na ₂ O	0.36	0.37	0.35	0.34	0.32	0.4	0.38	0.36	0.38	0.33	0.42
K ₂ O	n.d.	n.d.	0.02	0.01	n.d.	0.01	n.d.	n.d.	n.d.	0.01	0.01
Total	100.90	100.08	100.21	99.92	100.32	99.70	100.33	100.65	100.22	100.00	100.33
Si	1.877	1.877	1.891	1.894	1.901	1.885	1.893	1.884	1.869	1.860	1.883
Ti	0.011	0.015	0.013	0.011	0.013	0.021	0.018	0.017	0.031	0.031	0.017
Al	0.132	0.122	0.174	0.163	0.147	0.161	0.160	0.162	0.161	0.162	0.152
Al ^{VI}	0.009	0.000	0.066	0.057	0.048	0.046	0.053	0.046	0.030	0.022	0.034
Cr	0.029	0.030	0.027	0.030	0.025	0.025	0.026	0.026	0.023	0.039	0.023
Fe ³⁺	0.088	0.090	0.016	0.022	0.024	0.030	0.019	0.036	0.041	0.041	0.056
Fe ²⁺	0.095	0.051	0.127	0.132	0.100	0.103	0.114	0.101	0.089	0.125	0.082
Mn	0.004	0.004	0.005	0.006	0.003	0.004	0.003	0.004	0.005	0.006	0.006
Mg	0.957	0.875	0.916	0.916	0.864	0.849	0.861	0.852	0.864	0.912	0.918
Ca	0.781	0.909	0.804	0.802	0.902	0.892	0.879	0.894	0.888	0.801	0.833
Na	0.025	0.026	0.025	0.024	0.023	0.028	0.027	0.025	0.027	0.023	0.030
K	n.d.	n.d.	0.001	n.d.	n.d.	n.d.	n.d.	n.d.	n.d.	n.d.	n.d.
X(Mg)	0.91	0.94	0.87	0.87	0.89	0.89	0.88	0.89	0.90	0.87	0.91
Jd	0.91	0.00	2.56	2.45	2.26	2.90	2.69	2.54	2.69	2.19	3.00
Ac	1.62	2.62	n.d.	n.d.	n.d.	n.d.	n.d.	n.d.	n.d.	0.20	n.d.
Ca-Fe Tsc	5.07	4.67	2.15	2.60	2.44	2.78	2.25	3.06	3.24	3.90	3.93
Ca-Ti Tsc	1.06	1.51	1.29	1.10	1.26	2.13	1.84	1.72	3.13	3.09	1.72
Ca Tsc	5.07	4.57	6.14	5.81	4.94	4.48	4.82	5.11	3.60	3.90	4.36
Wol	33.47	40.09	35.42	35.35	40.76	39.92	39.50	39.73	39.44	34.60	36.66
En	47.85	43.77	45.82	45.79	43.19	42.43	43.05	42.62	43.22	45.59	45.90
Fs	4.96	2.76	6.62	6.89	5.15	5.36	5.86	5.22	4.68	6.53	4.43
Jd	0.91	n.d.	2.56	2.45	2.26	2.90	2.69	2.54	2.69	2.19	3.00
Ac	1.62	2.62	n.d.	n.d.	n.d.	n.d.	n.d.	n.d.	n.d.	0.20	n.d.
Aug	97.48	97.38	97.44	97.55	97.74	97.10	97.31	97.46	97.31	97.61	97.00

Jd – jadeite; Ac– acmite; Tsc– tschermakite; Wol– wollastonite; En– enstatite; Fs– ferrisilite

Table 3. Microprobe results for plagioclase from the Deli Jovan gabbros.

Sample	Fresh	Fresh	Fresh	Fresh	Fresh	Fresh	Fresh	Fresh	Fresh	Altered	Altered	Altered
	DJ-1	DJ-1	DJ-1	DJ-1	DJ-1	DJ-1	DJ-6	DJ-6	DJ-6	DJ-2	DJ-2	DJ-2
Comment	center	margin	center	margin	center	margin	center	center	center	–	–	–
SiO ₂	48.19	45.83	48.92	46.40	47.62	47.99	47.42	47.30	46.35	53.44	50.91	49.06
TiO ₂	n.d.	n.d.	n.d.	n.d.	n.d.	n.d.	n.d.	n.d.	n.d.	n.d.	n.d.	n.d.
Al ₂ O ₃	32.65	34.37	32.91	34.47	33.13	32.33	32.10	32.27	32.74	29.38	30.60	31.64
FeO	0.18	0.16	0.31	0.18	0.31	0.38	0.28	0.27	0.24	0.43	0.39	0.50
MnO	n.d.	n.d.	n.d.	n.d.	n.d.	n.d.	n.d.	n.d.	n.d.	n.d.	n.d.	n.d.
MgO	n.d.	n.d.	n.d.	n.d.	n.d.	n.d.	n.d.	n.d.	n.d.	n.d.	n.d.	n.d.
CaO	16.27	18.27	15.38	17.91	16.68	16.21	16.24	16.32	16.69	12.10	14.28	15.60
Na ₂ O	2.44	1.17	2.43	0.91	2.06	2.62	2.34	2.19	2.03	4.39	3.51	2.69
K ₂ O	0.01	0.02	n.d.	0.01	0.05	0.01	0.02	0.04	0.04	0.08	0.04	0.03
Total	99.74	99.82	99.95	99.88	99.85	99.54	98.44	98.42	98.13	99.82	99.73	99.52
Si	2.21	2.12	2.24	2.15	2.19	2.20	2.21	2.20	2.16	2.43	2.33	2.26
Ti	n.d.	n.d.	n.d.	n.d.	n.d.	n.d.	n.d.	n.d.	n.d.	n.d.	n.d.	n.d.
Al	1.77	1.87	1.78	1.88	1.79	1.75	1.76	1.77	1.80	1.57	1.65	1.71
Fe ²⁺	0.01	0.01	0.01	0.01	0.01	0.01	0.01	0.01	0.01	0.02	0.01	0.02
Mn	n.d.	n.d.	n.d.	n.d.	n.d.	n.d.	n.d.	n.d.	n.d.	n.d.	n.d.	n.d.
Mg	n.d.	n.d.	n.d.	n.d.	n.d.	n.d.	n.d.	n.d.	n.d.	n.d.	n.d.	n.d.
Ca	0.80	0.90	0.75	0.89	0.82	0.80	0.81	0.81	0.83	0.59	0.70	0.77
Na	0.22	0.10	0.22	0.08	0.18	0.23	0.21	0.20	0.18	0.39	0.31	0.24
K	n.d.	n.d.	n.d.	n.d.	n.d.	n.d.	n.d.	n.d.	n.d.	n.d.	n.d.	n.d.
X(Ca)	0.79	0.90	0.78	0.92	0.82	0.77	0.79	0.80	0.82	0.60	0.69	0.76
X(Na)	0.21	0.10	0.22	0.08	0.18	0.23	0.21	0.19	0.18	0.39	0.31	0.24
X(K)	0.00	0.00	0.00	0.00	0.00	0.00	0.00	0.00	0.00	0.00	0.00	0.00

X(Ca)– anorthite; X(Na)– albite; X(K)– orthoclase

quantify the effect of the plagioclase accumulation, a series of phase-equilibria calculations simulating the formation conditions of the Deli Jovan cumulates and adcumulates have been carried out.

Estimate of the Nature of Parent Melts of High-Al Gabbros of the Deli Jovan Massif: Application of the Geochemical Thermometry Method

Geological observations testify that the BCO sequence represents a uniform disintegrated MOR-type complex. The whole-rock compositions of the oceanic cumulate series (as is typical for that

sort of complex) differ markedly from those of the associated volcanics. This states the need to evaluate the composition of initial melts entrapped in these cumulates, as well as a genetic problem of the probable correspondence between the trapped liquids and parental magmas responsible for the formation of co-magmatic dykes and basalts. This problem is extensive enough and is outside the scope of this paper. So, it will be considered briefly with emphasis on the origin of high-Al gabbros to which all of the studied gabbroic samples belong. This goal will be accomplished by ‘*Geochemical Thermometry*’ (GT; Ariskin & Barmina 2004), a computer-based

Table 4. Whole rock composition of the studied samples from the Deli Jovan Complex: major elements.

	DJ-1-98	DJ-6-98	DJ-4-98	DJ-5-98	DJ-1b-03	DJ-1c-03
SiO ₂	46.93	44.29	47.85	44.51	45.99	48.15
TiO ₂	1.26	0.10	0.39	0.09	0.07	0.16
Al ₂ O ₃	13.85	19.04	22.51	23.28	24.43	22.54
FeO	11.78	6.17	6.50	6.06	4.40	4.59
MnO	0.25	0.10	0.10	0.09	0.07	0.07
MgO	9.36	15.65	6.48	12.55	6.75	6.48
CaO	10.44	10.70	10.50	9.42	13.57	13.90
Na ₂ O	1.95	0.82	3.02	1.54	1.32	1.37
K ₂ O	0.42	0.03	0.09	0.04	0.04	0.03
P ₂ O ₅	0.10	0.01	0.05	0.02	0.01	0.01
LOI	1.51	1.68	1.79	1.73	2.42	1.75
Total	99.16	99.28	99.28	99.32	99.07	99.05

Table 5. Whole rock composition of the studied samples from the Deli Jovan Complex: trace elements.

	DJ-1-98	DJ-6-98	DJ-4-98	DJ-5-98	DJ-1b-03	DJ-1c-03	Du-1c
Ba	84	6	71	22	31	20	7
Sr	169	132	144	130	156	130	164
Nb	1	1	2	2	1	n.d.	n.d.
Zr	78	5	25	14	13	16	10
Y	33	2	15	5	6	10	6
Pb	11	14	3	7	1	2	5
Cr	377	425	224	270	113	712	872
Ni	152	622	88	390	166	169	278
Co	53	62	35	62	29	31	41
V	266	27	142	20	13	52	69
Sc	37	5	27	17	19	25	n.d.

technique designed to extract principal information on the formation conditions of cumulates, including their initial temperature, composition of trapped liquid, compositions of primocryst minerals, and original modal proportions, as 'recorded' in the whole-rock chemistry. The GT-approach is based on the premise that any crystal mush (as a precursor of a completely crystalline rock) should pass through a

stage when relative motions of solids and magmatic melt have ceased, with cumulate crystals being, on average, in equilibrium with the trapped melt. The temperature of the equilibrated trapped liquid can be defined as the initial (parental) magma temperature. In this case, the initial cumulus mixture may be considered as a closed system, so that it becomes theoretically feasible to reconstruct all of the above

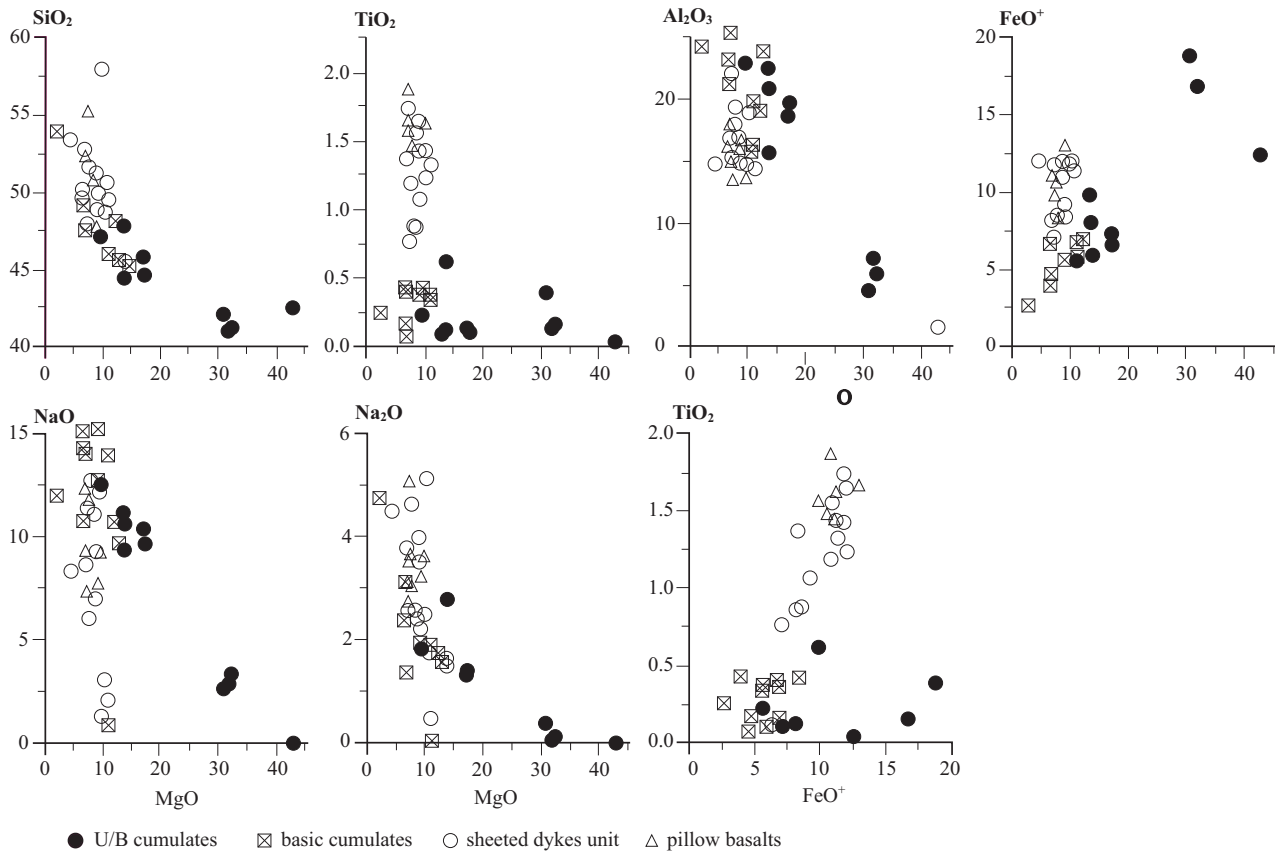


Figure 6. Variation diagrams of major elements of the BCO sequence.

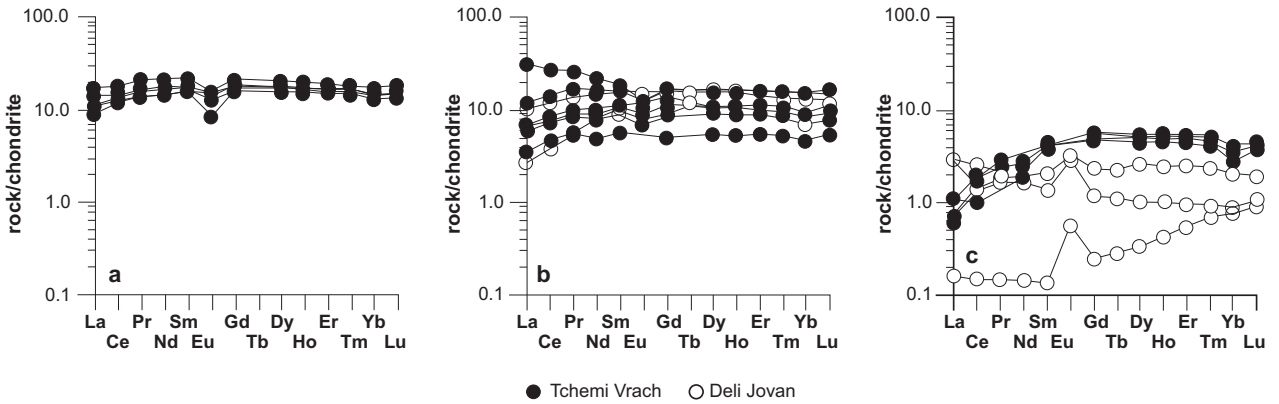


Figure 7. REE patterns for the BCO magmatic series: (a) lava flows; (b) dykes; (c) gabbroic cumulates (chondrite, Sun & McDonough 1989).

original characteristics based on inverse calculations simulating equilibrium melting/crystallization relations for corresponding naturally observed

cumulate rocks (Ariskin 1999). For this purpose at least two intrusive rocks must be available with differing bulk compositions due only to variations

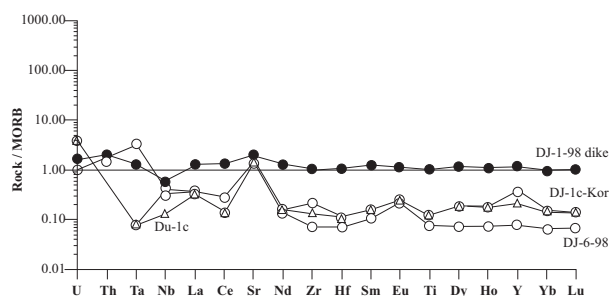


Figure 8. MORB-normalized multi-element patterns of the studied samples. Positive Sr and Eu anomalies and general depletion in trace element contents is characteristic for gabbroic rocks compared to diabase (MORB, Sun & McDonough 1989).

of the modal proportions of cumulus crystals, with the ‘trapped’ melt composition and its initial temperature being essentially the same. If this is true, one can state that during equilibrium melting of two or more samples which have been crystallized from the same ‘initial temperature’, the modelled liquid lines of descent (LLDs) will converge with falling temperature and intersect at a point that represents the conditions under which the assemblage had existed initially. Thus, to decipher the chemical record of the original cumulate pile equilibrium, one should: (1) select several samples for which the same initial cumulus conditions might be assumed, (2) conduct melting/crystallization modelling, including the chemical evolution of residual (assumed trapped) liquids, (3) display the calculated LLDs for each sample on T-X diagrams, and finally (4) identify an area of intersection or convergence of these lines that would approximate the assumed original cumulus equilibrium.

In practice, the numeric melting of selected rocks can be replaced with construction of crystallization trajectories for the same whole-rock compositions, as far as equilibrium crystallization is a reversible process with respect to the equilibrium melting. Hence, the Geochemical Thermometry of our gabbroic rocks was accomplished using the COMAGMAT-3.59 magma crystallization model (Ariskin & Barmina 2000, 2004). The program was developed to simulate crystallization of mafic to ultramafic magmas under a predetermined range of pressures and oxygen fugacity and its efficiency in conducting the GT-calculations. This approach has

been successfully tested on dolerite sills from the Siberian Platform (including the Talnakh Intrusion), hypabyssal rocks from the Kronotsky Peninsula (Eastern Kamchatka, Russia), the Skaergaard intrusion (Greenland), troctolites from the Partridge River intrusion (Duluth Complex, USA), and the Kiglapait troctolite Intrusion, (Labrador, Canada), see (Ariskin & Barmina 2004 and references therein).

Results of Geochemical Thermometry (Simulation of Phase Equilibria; 2kb, WM, Anhydrous) – Sixteen starting compositions including 8 real rocks and 8 weighted mean compositions characterizing the BCO sequence (Deli Jovan and Tcherni Vrah massifs; Savov *et al.* 2001) as a whole were used for the thermometric calculations. Five gabbroic samples from the Deli Jovan Massif (gabbros DJ-1b, DJ-1c, DJ-4, DJ-5, and DJ-6) are from the ‘homogenous gabbros’ level and can be considered as representatives of the uppermost part of the cumulate gabbro sequence. The diabase DJ-1-98 is considered to represent the volcanic section of the ophiolite complex. Two gabbros (GB-5, GB-20) are from the Tcherni Vrach Massif. The weighted mean data of the main units of the BCO represent high-Al troctolites of the lower cumulates, high-Al gabbros (upper cumulates), dykes and lava suites, respectively. These compositions were considered as an additional source of information on the emplacement temperatures and the compositions of original cumulate phases and parental magmatic melts. During GT-calculations with COMAGMAT, these average compositions were used in the same manner as those of the selected rock samples. The initial pressure, water content, and redox conditions for the modelled rocks were assumed to be similar to those of MORB from oceanic spreading zones. The oxygen fugacity was postulated to correspond to the Wustite-Magnetite buffer (approximately 1 log unit lower the Quartz-Fayalite-Magnetite buffer); H₂O content is of 0.1–0.2 wt%, with the total pressure ranging from 1 bar to 2kb (Christie *et al.* 1986; Danyushevsky 2001; Danyushevsky *et al.* 2004 and references therein). The equilibrium crystallization trajectories were calculated successively for each sample in a stepwise manner, with the crystal increment being 1 mol%. The maximum crystallinity of the modelled systems was assumed up to 90% (that correspond to 10% of liquid entrapped in cumulates). The main results of the COMAGMAT modelling are

summarized in Tables 6 & 7 and shown in Figure 9. The calculated arrival of minerals on the liquidus corresponds to initial melt compositions with a wide field of redundant plagioclase for most Al-enriched gabbros and an early crystallization of olivine for few high-Mg samples. After the excess crystallization

of Ol or Pl, both minerals start to crystallize simultaneously, followed by appearance of augite as the third cotectic mineral (the olivine+plagioclase+clinopyroxene assemblage). Note that seven of the high-Al gabbros demonstrate an essential excess of Pl crystallization (18–36 wt%) at high temperatures and only one gabbroic sample (DJ-6) indicates sub-cotectic (plagioclase+olivine) phase relations, after crystallization of a small amount of olivine (1–9 wt%; see Table 8). Furthermore, it is important to realize that the melting-crystallization relationships do not refer to any real magma temperatures; they just demonstrate different amounts of accumulation of plagioclase and olivine crystals in the modelled cumulate. In order to evaluate the likeliest range of initial (probably cotectic) magma temperatures and compositions, one should utilize additional information, which is obtained from the ‘behaviour’ of the calculated liquid lines of descent displayed together on the temperature-composition diagrams. The modelled liquid lines of descent (LLDs) in terms of the calculated temperatures (as approximation of the probable trapped liquid evolution) are shown in Figure 9. Note that in the high-Al gabbros these trajectories can be attributed with a high degree of confidence to a single genetic ‘family’ of modelled liquids that converge in the T-X space to produce the same Ol-Pl cotectics. A similar type of modelled liquids was obtained for more magnesian high-Al troctolites from the ‘lower cumulates’ of the Tcherni Vrah Massif. This argues that the selected compositions represent a genetically uniform magmatic sequence,

Table 6. Whole rock composition of the studied samples from the Deli Jovan Complex: U, Th, Ta, Hf and REE.

	DJ-1-98	DJ-6-98	DJ-1c-03
U	0.08	0.05	0.18
Th	0.23	0.18	n.d.
Ta	0.18	0.43	0.01
Hf	2.11	0.15	0.23
La	3.17	0.93	0.84
Ce	9.79	2.05	1.06
Pr	1.69	0.24	0.20
Nd	9.28	1.03	1.15
Sm	3.17	0.28	0.41
Eu	1.14	0.22	0.25
Gd	4.27	0.32	0.63
Tb	0.77	0.05	0.11
Dy	5.11	0.34	0.85
Ho	1.11	0.07	0.18
Er	3.15	0.20	0.54
Tm	0.46	0.03	0.08
Yb	2.96	0.20	0.45
Lu	0.45	0.03	0.06

Table 7. Characteristic intervals of crystallization trajectories of the high-Al gabbros from the Deli Jovan Massif.

	Excess Pl	Ol-Pl cotectics	Addition of Cpx
DJ-1b-03	T= 1429.6–1274.8°C Pl _{97.4} –Pl _{91.2}	T= 1270.3–1198.2°C Ol _{90.8} Pl _{90.9} –Ol _{82.8} Pl _{81.5}	T= 1195.0°C Ol _{82.5} Pl _{80.9} +Cpx
DJ-1c-03	T= 1398.6–1245.4°C Pl _{96.4} –Pl _{88.6}	T= 1241.757–1210.03°C Ol _{89.813} Pl _{88.4} –Ol _{86.7} Pl _{84.6}	T= 1208.343°C Ol _{86.5} Pl _{84.4} +Cpx
Al-gabbro average	T= 1355.30–1276.02°C Pl _{93.2} –Pl _{87.2}	T= 1271.12–1188.01°C Ol _{91.05} Pl _{86.7} –Ol _{80.8} Pl _{68.4}	T= 1187.67°C Ol _{80.4} Pl _{69.2} +Cpx
DJ-6-98	T= 1367.126–1292.073°C Ol _{94.4} –Ol _{92.9} (almost cotectic)	T= 1290.113–1198.151°C Ol _{92.9} Pl _{95.7} –Ol _{83.7} Pl _{85.4}	T= 1195.028°C Ol _{83.6} Pl _{85.1} +Cpx

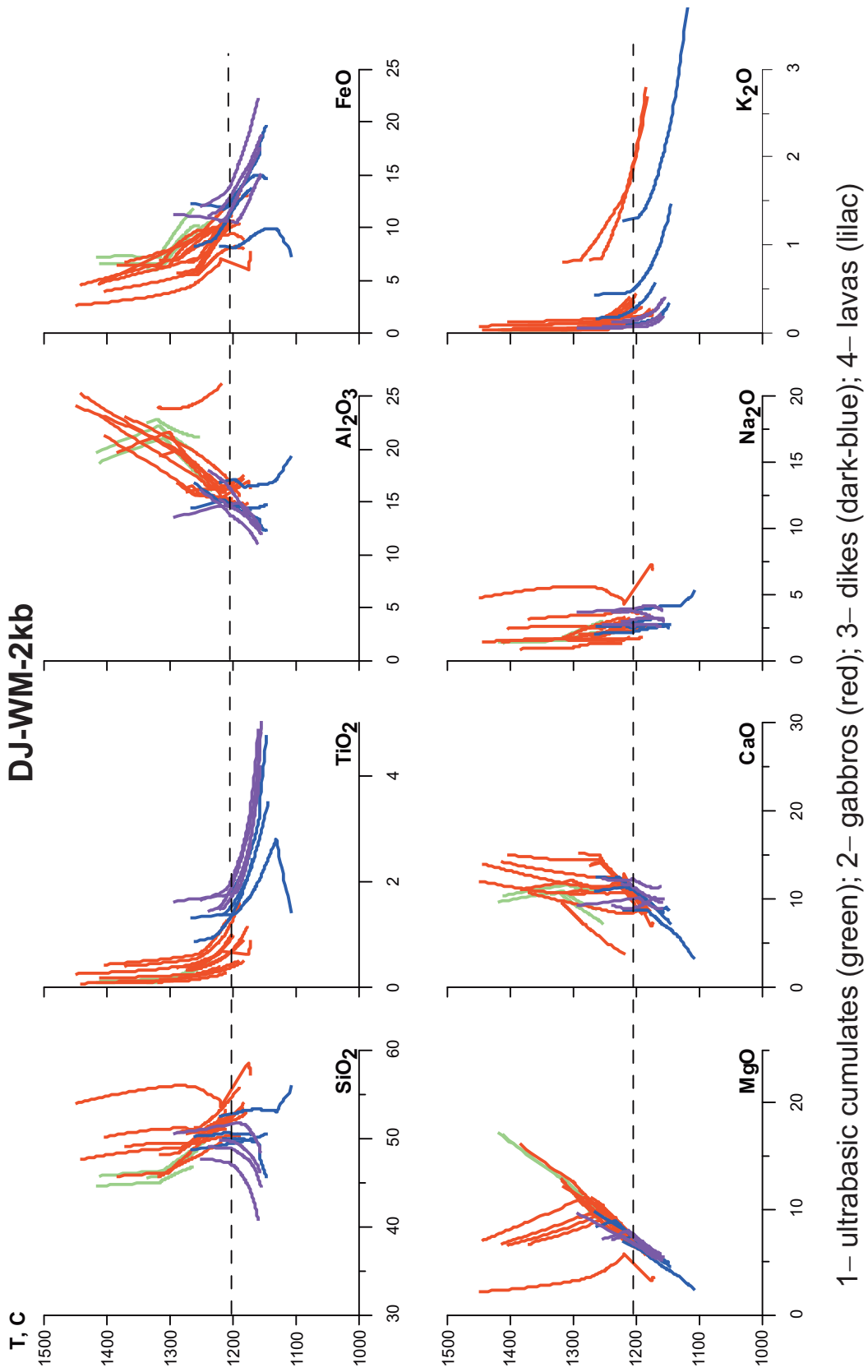


Figure 9. Equilibrium crystallization curves of the Balkano-Carpathian ophiolitic sequences.

Table 8. Trapped melt compositions calculated for typical high-Al gabbros from the Deli Jovan Massif.

Sampl	Temperature °C	SiO ₂	TiO ₂	Al ₂ O ₃	FeO	MnO	MgO	CaO	Na ₂ O	K ₂ O	P ₂ O ₅	Mg# of the melt	Fo, mole%	An, mole%	En in Aug, mole%	Fs in Aug, mole%	Wo in Aug, mole%	Al ₂ O ₃ In Aug, wt%	
Sample DJ-1b-03																			
1360	48.42	0.091	22.55	5.73	0.09	8.78	12.70	1.58	0.05	0.013	0.73	95.2							
1275	48.93	0.114	19.54	7.18	0.11	11.00	11.46	1.61	0.06	0.016	0.73	91.2							
1270	48.95	0.116	19.36	7.28	0.11	11.11	11.40	1.60	0.06	0.017	0.73	90.9							
1205	52.62	0.242	15.50	9.88	0.16	8.16	11.68	1.60	0.12	0.035	0.60	83.4	82.5						
1195	53.34	0.268	14.92	9.99	0.16	7.79	11.81	1.56	0.13	0.038	0.58	82.5	80.9	42.0	8.9	49.1	41.1	3.2	
Sample DJ-1c-03																			
1344	50.37	0.194	20.92	5.56	0.08	7.85	13.43	1.55	0.04	0.012	0.72	94.3							
1283	51.03	0.225	18.71	6.47	0.10	9.13	12.74	1.57	0.04	0.014	0.72	91.0							
1191	54.45	0.414	15.19	9.40	0.13	7.61	11.21	1.49	0.08	0.029	0.59	83.0	81.8	50.1	8.8	41.1	3.2		
Sample DJ-6-98																			
1290	46.15	0.114	21.55	6.36	0.10	12.62	12.12	0.94	0.03	0.011	0.78	92.9							
1280	46.91	0.146	20.66	7.27	0.12	11.96	11.80	1.08	0.04	0.015	0.75	91.5	94.6						
1251	48.90	0.239	18.64	8.95	0.15	10.34	11.41	1.28	0.07	0.024	0.67	88.0	91.3						
1195	53.43	0.475	15.30	9.44	0.16	7.99	11.80	1.24	0.12	0.048	0.67	83.6	85.0	59.00	8.4	41.6	3.10		

Fo- forsterite; An- anorthite; En- enstatite; Fs- ferrisillite; Wo- wollastonite; Aug- augite.

and simultaneously demonstrates an ability to evaluate both the range of cotectic magma temperatures and trapped melt compositions recorded in the Pl-cumulate compositions. Based on consideration of the individual plots in Figure 9, we believe the SiO_2 -T, Al_2O_3 -T, FeO-T, MgO-T, and CaO-T diagrams are reliable enough to perform the GT-analysis, whereas the TiO_2 -T diagram is a useful tool to separate samples representing more primitive and more evolved magmatic material, probably of two different magma types. On temperature-concentration diagrams (Figure 9), a convergence and intersection of modelled liquid compositions below 1300°C is displayed. This pattern is consistent with the premise that the selected cumulates are really mechanical mixtures of cumulus crystals and entrapped parental melts. The most probable temperature range of the parental magmas for the BCO high-Al gabbros might be constrained at 1190 – 1270°C . The lowest value corresponds to the upper temperature limit of the modelled onset of crystallization of clinopyroxene (assuming the 'low-temperature' assemblage $\text{Ol}_{83-84} + \text{Cpx}_{84-87} + \text{Pl}_{77-82}$), whereas the highest possible temperature corresponds to the transition area between the crystallization of excess plagioclase and the olivine-plagioclase cotectic (constrained by the Pl_{91-92} compositions measured in the samples DJ-1b-03 and DJ-1c-03). The most compact cluster of the T-X crystallization trajectories (for gabbroic compositions) seems to exist in the interval of 1190 – 1220°C . At these temperatures, the modelled (parental) melts correspond to silica saturated, low-Ti, and low-K magmas of fractionated (mg# 0.60–0.58) tholeiitic basalts. Liquidus assemblages modelled at the highest temperatures ($> 1250^\circ\text{C}$), containing anorthitic plagioclase (Pl_{91-92}), crystallized from more magnesian (mg# 0.73) and obviously high-Al (> 18 wt% Al_2O_3) melt with lower contents of TiO_2 and alkalis. A series of melts modelled at different temperatures for several representative samples (DJ-1b-03, DJ-1c-03, and DJ-6-98) are shown in Table 7. Coupled with plots in Figure 9, these data illustrate a consecutive transition from higher temperature high-Al melts to those corresponding to lower temperature normal aluminous gabbros. We interpret this transition as a result of equilibrium crystallization and abundant separation and/or accumulation of plagioclase (up to 40 %), followed by cotectic

crystallization of plagioclase and olivine. When the TiO_2 -T diagram in Figure 9 is used, a certain gap between the modelled LLDs for the high-Al gabbros and those of associated volcanics (dykes and lavas) is observed. This is clearly revealed by the crystallization trajectory of the dolerite dyke liquids (DJ-1-98), that are drastically different from the whole set of the gabbroic curves. At temperatures at or below 1200°C , the probable dolerite melts correspond to those slightly undersaturated with silica, moderate to high-Ti and low-K tholeiitic basalts, that are obviously more evolved than the associated gabbros (Tables 6 & 7). Assuming the DJ-1-98 sample to be representative for the whole volcanic complex, one can conclude the uppermost volcanic part of the BCO was formed by more evolved and fractionated magmas than the underlying cumulate sequence.

Conclusions from GT Modelling – Comparison of the calculated compositional variations of the liquidus minerals with results from microprobe studies of the selected gabbros (mostly the bimodal distribution of Pl compositions) allows two basic intervals of crystallization of their parental melts to be defined. The established anorthite composition (Pl_{91-92}) relates to a high-temperature stage of transition from crystallization of the redundant plagioclase to cotectic crystallization of plagioclase and olivine. Nevertheless, the real existence of such high-temperature high-Al melts for gabbroic cumulates of the Deli Jovan Massif should be considered problematic, as the expected high magnesium olivine Fo_{90-91} in equilibrium with anorthitic plagioclase (Pl_{91-92}) has not really been established. The composition of the less calcic plagioclase (Pl_{77-82}) is consistent with crystallization of a lower temperature cotectic ($\text{Ol} \pm \text{Pl} \pm \text{Cpx}$), near an inflection point, where CaO content in the melt begins to decrease due to appearance of clinopyroxene in the liquidus of more evolved residual magma. In connection with the results it is necessary to note that the high-Al basaltic melt inclusions are reliably established in the setting of oceanic spreading zones (Nielsen *et al.* 1995; Danyushevsky *et al.* 2003, 2004 and references therein). These melt inclusions are characterized by unusually low contents of incompatible elements and strong Sr and moderate positive Eu anomalies. Trace element patterns of such type are very similar to those of some plagioclase-rich oceanic

troctolites and are related to localized dissolution of earlier formed gabbroic ‘cumulates’ within the crustal mush zone, while the hot primitive MORB-type magma was passing through (Danyushevsky *et al.* 2003). Interestingly, at the same time this assimilation process appears to have little effect on the compositions of erupted MORB, because there is a lack of an assimilation signature in associated volcanics. The calculated compositions of high-Al melts, the established features of trace element patterns of the cumulate gabbros and associated volcanics, and also the isotope ratios of Nd and Sr (see below) in gabbroic series of the palaeo-oceanic complex of Deli Jovan, support this model.

Regional Metamorphic Overprints on the Deli Jovan Gabbroic Cumulates

Samples DU-2-03 and DJ-4-98 are altered gabbros. Data on their metamorphic mineral assemblages are presented in Tables 8 & 9 and Figures 10 & 11.

In sample *DU-2-03* alteration is expressed in the formation of actinolite (hornblende)-chlorite-epidote rims, or full pseudomorphs of the same composition on clinopyroxene, and occurrence of a series of veinlets of chlorite-epidote and carbonate. Initially, replacement of clinopyroxene by the thinnest segregations of actinolite occurs along cleavage planes, with the formation of small epidote-chlorite selvages

Table 9. Change of composition of Ca-amphibole from concentric amphibole-chlorite-epidote pseudomorph on Cpx in gabbro from the Deli Jovan Massif – a profile from actinolite core to Chl-Ep±Prg rim (sample DU-2-03).

point of analysis	middle amphibole part of pseudomorph					outer Chl-Ep-Prg rim	
type of grain	from center to margin					euhedral inclusions in Ep	
SiO ₂	58.16	57.81	57.23	56.88	52.29	44.00	42.49
TiO ₂	n.d.	n.d.	0.11	0.05	n.d.	0.21	n.d.
Al ₂ O ₃	0.04	0.03	0.31	0.57	5.23	14.93	16.98
FeO	3.32	4.30	5.72	8.40	8.32	10.54	10.70
MnO	0.18	0.18	0.15	0.14	0.06	0.02	n.d.
MgO	22.37	22.21	21.24	19.05	19.64	13.20	13.02
CaO	13.55	12.73	13.11	12.83	11.04	12.34	11.84
Na ₂ O	0.22	0.31	0.19	0.20	0.90	2.92	3.23
K ₂ O	n.d.	0.09	0.01	0.04	0.02	0.06	0.16
Total	97.84	97.66	98.07	98.16	97.50	98.22	98.42
23 O							
Si	7.99	7.99	7.94	7.96	7.33	6.33	6.10
Al ^{IV}	0.01	0.01	0.06	0.04	0.67	1.67	1.90
Al ^{VI}	0.01	n.d.	n.d.	0.05	0.19	0.86	0.97
Ti	n.d.	n.d.	0.01	0.01	n.d.	0.02	n.d.
Fe ³⁺	0.02	n.d.	n.d.	0.03	0.45	0.16	0.29
Fe ²⁺	0.36	0.50	0.66	0.96	0.52	1.10	0.99
Mn	0.02	0.02	0.02	0.02	0.01	n.d.	n.d.
Mg	4.58	4.57	4.39	3.97	4.10	2.83	2.78
Ca	1.99	1.88	1.95	1.92	1.66	1.90	1.82
Na	0.06	0.08	0.05	0.05	0.24	0.81	0.90
K	n.d.	0.02	n.d.	0.01	n.d.	0.01	0.03
Fe ²⁺ /Fe ²⁺ +Mg	0.07	0.10	0.13	0.19	0.11	0.28	0.26
(Na+K) _A	0.05	0.07	0.05	0.01	0.13	0.74	0.81
Amphibole	Act	Act	Act	Act	Mg-Hb	Prg	Prg

Act– actinolite; Mg-Hb– Mg-hornblende; Prg– pargasite

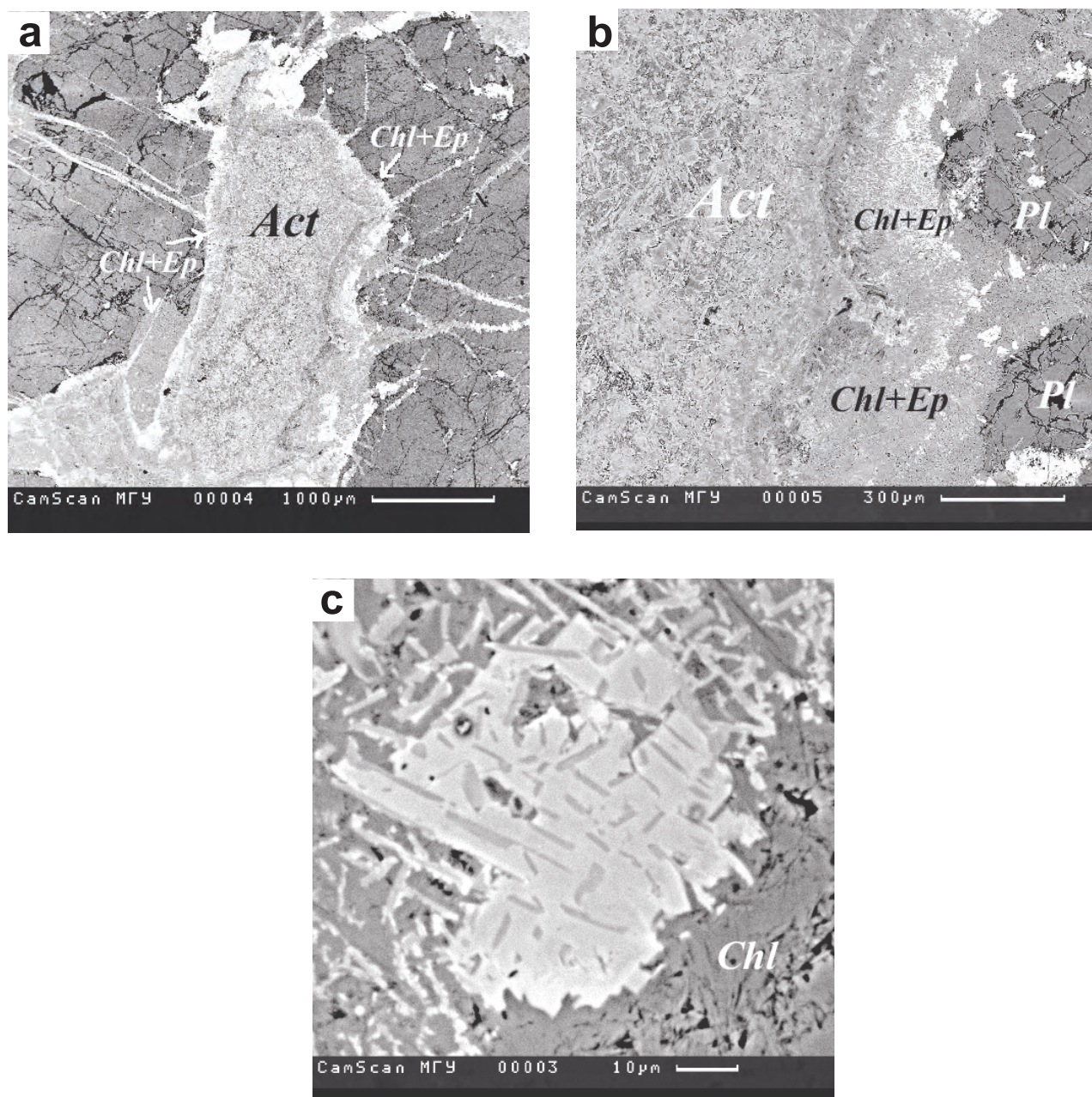


Figure 10. Typical microphotographs of altered Deli Jovan gabbros. The primary clinopyroxene-plagioclase association is irregularly replaced by the paragenesis of actinolite-hornblende-chlorite-clinozoisite. (a) Three-zones pseudomorph on clinopyroxene: actinolite (core) → hornblende (pargasites) → epidote+chlorite±hornblende (rim) from the centre of replaced clinopyroxene to its contact with plagioclase; (b) Three-zone pseudomorph on clinopyroxene; (c) Equilibrium intergrowth of epidote and pargasite (dark-grey prisms) in the assemblage of the outer epidote-chlorite-pargasite rim.

in contact with clinopyroxene and plagioclase. The metamorphism concludes with full actinolite (hornblende)-chlorite-epidote pseudomorphs of clinopyroxene, to which epidote-chlorite and carbonate veinlets approach (feeding channels of

fluids; Figure 10a). All pseudomorphs are zoned – the core is exclusively actinolite (Figure 10b), while the outer rim, in contact with plagioclase, is composed of an assemblage of chlorite-epidote±hornblende. From the actinolite core, to external chlorite-

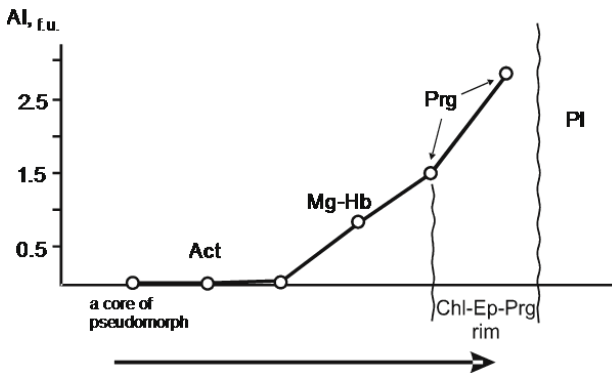


Figure 11. Modification of Ca-amphibole composition (f.u. formula units) from zoned pseudomorphs on clinopyroxene, from centre to margin.

epidote-hornblende rim contents of Fe and Al of pseudomorphous Ca-amphiboles increases (Table 9). Actinolite is replaced by common hornblende, so they form a sequence- Actinolite → Magnesian hornblende → Pargasite (a prograde tendency in the process of growth of pseudomorphs). Pargasites (Prg) most strongly enriched in Fe and Al are found as tiny prismatic inclusions (dark grey prisms) within the light grey epidote crystals at the epidote-chlorite-hornblende rim (Figure 10c.) Epidotes are also zoned (clinzoisite core and more iron-rich margins, Table 9). The prograde change of amphibole composition towards the external part of the pseudomorph (Figure 11) is caused by temperature increase and proves that the replacement of pyroxenes occurred during prograde greenschist facies metamorphism. The paragenesis formed specifies a temperature of c. 400–450°C (Spear 1995). At the same time the process was not completely in equilibrium, since magmatic plagioclase in contact reaction with clinopyroxene is not replaced by albite-oligoclase or saussurite but only by labradorite (Table 3).

The primary magmatic association in *Sample DJ-4-98 (amphibolized gabbro)* is plagioclase+clinopyroxene. The clinopyroxene is extensively replaced by actinolite; between crystals of plagioclase and clinopyroxene the association actinolite+chlorite+epidote-Fe-oxide is developed.

Results of Isotopic Research

Zircons by SHRIMP—The average grain size of zircons from gabbro DU-2-03 is 150–300 nm. The crystals

are transparent and pale yellowish. The overwhelming majority (95%) of the grains is represented by xenomorphic fragments of large crystals, but includes also (about 5%) more idiomorphic crystals of elongated prismatic shape with length/width ratio of 2:1. They are internally zoned and do not include any xenocrysts of other minerals. The cathode-luminescence image of most grains shows distinct sectoral magmatic zonation, characteristic for zircons in basic magmatic rocks. More idiomorphic crystals are characterized by a weak cathode-luminescence glow and the presence of fine magmatic zoning (Figure 12a, b). Thus, regardless of superimposed metamorphism, the primary magmatic zircon in high-Al gabbro DU-2-03 is well preserved.

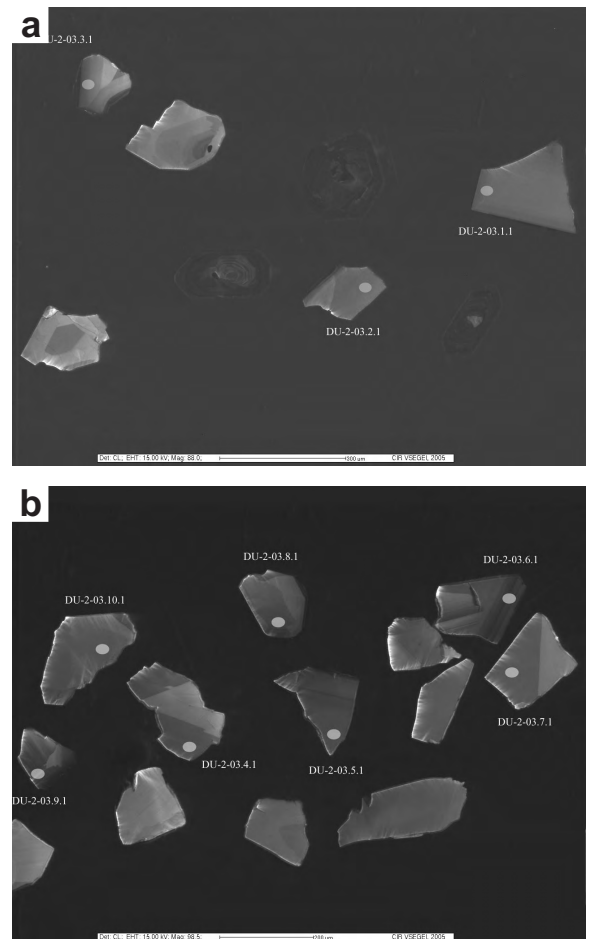


Figure 12. Cathode-luminescence image of zircons of gabbro DU-2-03, from gabbroic cumulates of the Deli Jovan Massif.

All measured zircon grains have $^{206}\text{Pb}/^{238}\text{U}$ ages ranging from 393.6–409.9 Ma with a mean at 405 ± 2.6 Ma (MSWD of concordance is 0.36); probability of concordance is 0.55. (Figure 13). The characteristic contents of U= 16–191 ppm, Th= 7–80 ppm, and Th/U= 0.35–0.67, were established. The unique higher content of U and Th (U= 388 ppm, Th= 242 ppm) in point 6.1. of sample DU-2-03 (Figure 13a), is located in the darker marginal part of the zircon grain. Measurements of finely zoned more euhedral crystals were not performed.

The *Sm-Nd Mineral Isochron* of high-Al gabbro DJ-6-98 (Table 10a, Figure 14) has yielded an age of 406 ± 24 Ma, coincident with the SHRIMP data from the gabbro DU-2-03 (Table 11, Figure 13). Age corrected isotopic ratios of Nd and Sr in the

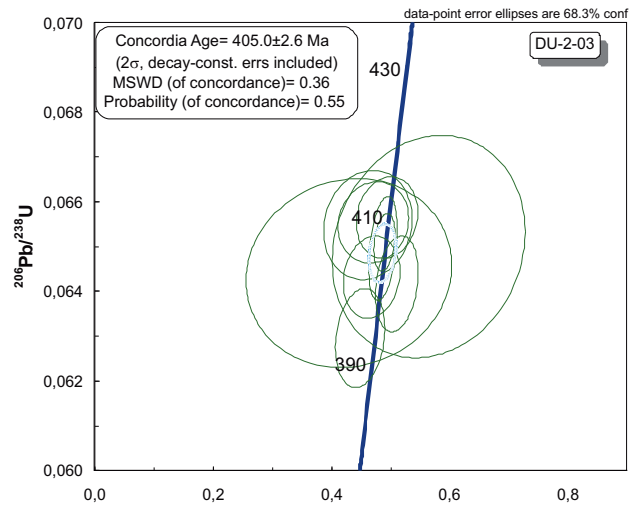


Figure 13. Concordia diagram of the Deli-Jovan gabbro DU-2-03.

Table 10. Microprobe data for epidote and chlorite from the outer part of an Amph-Chl-Ep pseudomorph in Cpx in gabbros from the Deli Jovan Massif.

	Epidote			Chlorite	
	center	rim			
SiO ₂	39.14	38.69	38.46	28.52	28.82
TiO ₂	0.05	0.04	0.05	0.10	n.d.
Al ₂ O ₃	28.34	25.81	25.04	21.11	20.86
Fe ₂ O ₃	6.54	9.90	11.70	n.d.	n.d.
FeO	n.d.	n.d.	n.d.	18.15	17.94
MnO	0.19	0.12	0.06	0.07	0.24
MgO	0.20	0.04	n.d.	21.19	21.21
CaO	23.82	23.48	23.24	0.14	0.05
Na ₂ O	0.08	0.04	0.18	0.36	n.d.
K ₂ O	0.05	n.d.	n.d.	0.06	0.07
Total	98.41	98.12	98.73	89.70	89.19
	12.5 O			14 O	
Si	3.04	3.03	3.01	2.82	2.85
Al	2.60	2.38	2.31	2.45	2.43
Ti	n.d.	n.d.	n.d.	0.01	n.d.
Fe ³⁺	0.42	0.58	0.69	n.d.	n.d.
Fe ²⁺	n.d.	n.d.	n.d.	1.50	1.48
Mn	0.01	0.01	n.d.	0.01	0.02
Mg	0.02	n.d.	n.d.	3.12	3.13
Ca	1.99	1.97	1.95	0.01	0.01
Na	0.01	0.01	0.02	0.07	n.d.
K	n.d.	n.d.	n.d.	0.01	0.01
Fe ²⁺ /Fe ²⁺ +Mg				0.32	0.32
X _{Fe} ³⁺	0.14	0.20	0.23		

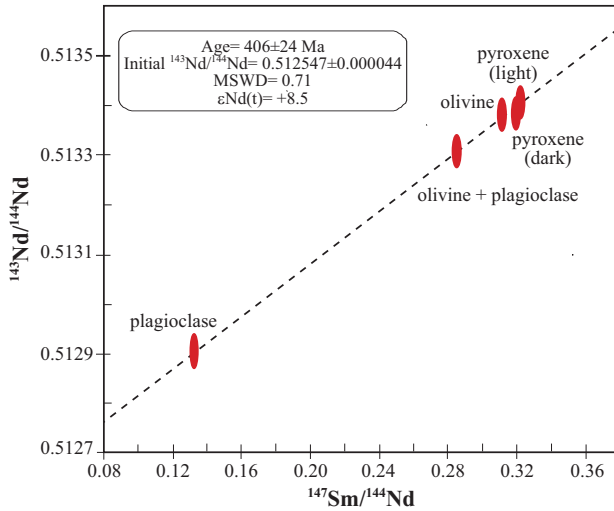


Figure 14. Sm-Nd mineral isochron of the Deli Jovan gabbro DJ-6-98. Ol- Olivine, Pl- Plagioclase, Px- pyroxene.

samples are for the high-Al gabbro DJ-6-98 $\epsilon Nd_{init} = +8.5$; $^{87}Sr/^{86}Sr_{init} = 0.702592$; $T_{DM} = 406$ Ma; and for the diabase dike DJ-1-98 $\epsilon Nd_{init} = +7.55$; $^{87}Sr/^{86}Sr_{init} = 0.702677$. This definitely specifies the relationship of their magmatic protoliths with a depleted mantle source (DMM, Zindler & Hart 1986; Hofman 1997). This interpretation agrees with the petrological and geochemical identification of these series as being of MORB type. The combined Sm-Nd mineral and WR isochron (DJ-1-98 diabase dyke and gabbro DJ-6-98) gave a less accurate age of 423 ± 46 Ma. Thus, inclusion of a figurative point of the volcanic rock (diabase DJ-1-98) does not disturb the received Sm-Nd isochron. Note that the calculated depleted mantle model age (T_{DM} ; Goldstein *et al.* 1984) for high-Al gabbro DJ-6-98 coincides with ages obtained by SHRIMP and Sm-Nd isochron methods. Correct calculation of the T_{DM} value for diabase dyke DJ-1-98 is precluded by its $^{147}Sm/^{144}Nd$ ratio (0.2145 ± 0.0002) coincident with that of depleted mantle reservoir.

Correlation of the Early-Middle Palaeozoic Oceanic Events of the BCO and Palaeo-Oceanic Zones of the Great Caucasus: A Discussion

(1) The study of the Deli Jovan Ophiolite Massif shows that within the Balkan-Carpathian ophiolite suture (BCO), situated between the Moesian Platform in the north and the Rhodope and Serbo-Macedonian massifs in the south (Thracian terrane),

Table 11. U-Pb isotopic data from the ion microprobe spot dating (SHRIMP) of zircons in high-Al gabbro DU-2-03 from the Deli Jovan massif (NE Serbia).

Spot	% ²⁰⁶ Pb _c	Ppm U	Ppm Th	Ppm ²³² Th/ ²³⁸ U	Ppm ²⁰⁶ Pb*	(1) Age ²⁰⁶ Pb/ ²³⁸ U	(1) Age ²⁰⁷ Pb/ ²³⁵ Pb	% Discordant	(1) ²³⁸ U/ ²⁰⁶ Pb	±%	(1) ²⁰⁷ Pb/ ²⁰⁶ Pb	±%	(1) ²⁰⁷ Pb/ ²³⁸ U	±%	(1) ²⁰⁶ Pb/ ²³⁸ U	±%	error correction
DU-2-03-4.1	0.58	64	33	0.54	3.47	393.6±4.4	268±140	-32	15.88	1.2	0.0516	6.1	0.448	6.2	0.06296	1.2	0.187
DU-2-03-5.1	n.d.	123	52	0.44	6.73	400.9±4.3	517±100	29	15.58	1.1	0.0577	4.6	0.51	4.7	0.06417	1.1	0.235
DU-2-03-9.1	0.51	129	62	0.50	7.15	401.8±3.7	317±150	-21	15.55	0.94	0.0527	6.7	0.468	6.8	0.06432	0.94	0.139
DU-2-03-7.1	1.53	32	17	0.56	1.79	402.4±8.4	115±630	-71	15.53	2.2	0.048	27	0.43	27	0.0644	2.2	0.081
DU-2-03-2.1	0.00	123	67	0.57	6.85	405.7±4.6	385±69	-5	15.39	1.2	0.0543	3.1	0.487	3.3	0.06496	1.2	0.359
DU-2-03-10.1	0.33	16	7	0.45	0.877	406±9.9	706±400	74	15.38	2.5	0.063	19	0.56	19	0.065	2.5	0.132
DU-2-03-6.1	0.02	388	242	0.65	21.7	406.5±2.6	392±52	-4	15.362	0.65	0.0545	2.3	0.489	2.4	0.0651	0.65	0.270
DU-2-03-1.1	0.71	71	46	0.67	4.05	408.9±4.9	245±250	-40	15.27	1.2	0.0511	11	0.461	11	0.06548	1.2	0.115
DU-2-03-3.1	0.22	191	65	0.35	10.8	409.2±3.6	289±190	-29	15.26	0.91	0.0521	8.3	0.471	8.4	0.06554	0.91	0.109
DU-2-03-8.1	0.04	165	80	0.50	9.3	409.9±3.6	394±150	-4	15.23	0.91	0.0545	6.9	0.494	6.9	0.06565	0.91	0.132

Errors are 1-sigma; Pb_c and Pb* indicate the common and radiogenic portions, respectively. Error in Standard calibration was 0.38%. (1) Common Pb corrected using measured ²⁰⁴Pb

Table 12. Sm-Nd and Rb-Sr isotopic results from the Deli Jovan massif (NE Serbia).

Sample	$^{147}\text{Sm}/^{144}\text{Nd}$	$^{143}\text{Nd}/^{144}\text{Nd}$
DJ-6 Plag	0.1328±0.0004	0.512900±0.000019
DJ-6-98 WR	0.1788±0.0001	0.512999±0.000025
DJ-1-98 WR	0.2145±0.0002	0.513067±0.000032
DJ-6 Ol+Pl	0.2856±0.0002	0.513310±0.000021
DJ-6 Ol	0.3114±0.0002	0.513387±0.000025
DJ-6 Px dark	0.3200±0.0002	0.513384±0.000006
DJ-6 Px light	0.3219±0.0002	0.513407±0.000019

Sample	$^{87}\text{Rb}/^{86}\text{Sr}$	$^{87}\text{Sr}/^{86}\text{Sr}$
DI-1b-98-WR	0.0245±0.00036	0.702817±0.000350
DI-6-98-WR	0.006±0.00009	0.702459±0.000351
Ap (6-98)	0.0138±0.00021	0.702597±0.000351

an Early Devonian oceanic event is evident. The geological setting of this event certainly corresponds to conditions of oceanic spreading zones, with magmatic sources matching depleted MORB mantle (DMM; Zindler & Hart 1986; Hofman 1997), high-Al gabbro DJ-6-98; ($\epsilon\text{Nd}_{\text{init}} = +8.03 / +8.5$; $^{87}\text{Sr}/^{86}\text{Sr}_{\text{init}} = 0.702592$; $T_{\text{DM}} = 406$ Ma) and diabase dyke DJ-1-98 ($\epsilon\text{Nd}_{\text{init}} = +7.55$; $^{87}\text{Sr}/^{86}\text{Sr}_{\text{init}} = 0.702677$).

In spite of the fact that formation mechanisms of the associated cumulate and volcanic series of the massif somewhat differ (see the above petrological identification of the high-Al gabbroic rocks), the origin of these series undoubtedly corresponds to some uniform oceanic lithosphere formation (Natland & Dick 2001; Danyushevsky *et al.* 2003).

(2) The Neoproterozoic–Early Cambrian age of the oceanic lithosphere of the BCO suture has been soundly substantiated by geological observations, biostratigraphic and geochronological data (Haydoutov & Yanev 1997; Haydoutov *et al.* 1996–1997; von Quadt *et al.* 1998; Savov *et al.* 2001; Carrigan *et al.* 2005 and references therein). According to a widely accepted concept put forward in these works the destruction of this oceanic basin between the Protomoesian and Thracian terranes occurred in the Early Ordovician. At the same time, it was assumed

that the Balkan, Sredna Gora and possibly parts of the Rhodope Massif were probably attached to southern Europe (Moesian terrane) during the Hercynian Orogeny (Yanev 2000; Haydoutov & Yanev 1997; Carrigan *et al.* 2005) although, the timing of this amalgamation is still not clearly known, in particular in the interval from the Ordovician to the Permian.

(3) The geochronological data obtained from the Deli Jovan Massif, obviously do not match this model. These data should increase our knowledge about the evolution of the European Palaeomargin in the Middle Palaeozoic, preceding the large-scale Hercynian orogenic events. Although problems of the origin of the Middle Palaeozoic and in particular the Devonian oceanic basins within the Central European Hercynides were discussed in a series of publications (Pin 1990; Matte 1991; von Raumer *et al.* 2002; Dal Piaz *et al.* 2003; Kebede *et al.* 2005; Kalvoda *et al.* 2008 and references therein), it remains difficult to specify direct analogues of Devonian oceanic events of the BCO in the Central European Hercynides, although Schulz *et al.* (2004) suggested indications for the opening of Palaeotethys (430 Ma) in the Austroalpine basement of the Eastern Alps, exactly on the western extension of the BCO. In the eastern extension of the BCO in the Great Caucasus pre-Hercynian Early–Middle Palaeozoic events of oceanic type are clearly present. A short outline of these most significant relevant data is given below.

Early–Middle Palaeozoic Oceanic Complexes of the Fold-Thrust Belt of the Great Caucasus: a Review

The region of the Caucasus is subdivided into two large geological provinces (Adamia *et al.* 1981). *The Southern Province* (South Armenian Subplatform SAS) a peri-Gondawanian block forming a NW extension of Central Iran. Pan-African (Cadomian) tectonic events are clearly shown, followed during the whole Palaeozoic (Cm, S-D-C-P) by accumulation of predominantly shallow-water marine deposits, carbonates and terrigenous classic sediments.

The Northern Province (the Caucasian Hercynides) is characterized by extensive Caledonian and, in particular Hercynian tectono-magmatic events, supra-subduction magmatism, strong regional

metamorphism and emplacement of granites (Adamia *et al.* 1987; Zakariadze *et al.* 2007). Rocks of pre-Mesozoic oceanic basins in the region, as a rule, are closely associated with granite-gneiss-migmatite complexes of Precambrian (Southern Province) and Precambrian-Palaeozoic (Northern Province) age.

The boundary between these provinces coincides with the Northern Anatolian (İzmir-Ankara-Erzincan)-Lesser Caucasus (Sevano-Akera) ophiolite belt (Adamia *et al.* 1981).

The Caucasus Mountains and the southern margin of the Scythian Platform contain numerous fragments of oceanic lithosphere, usually significantly dismembered and metamorphosed. As in the Balkan-Carpathian oceanic suture, these complexes are situated close to the transition zone of the Eastern European Hercynides to the European Platform. The largest exposures of metamorphosed accretionary mafic complexes are known along southern edge of the Hercynian Granite-Gneiss Core and also in Foreland Zones of the Great Caucasus (Figures 15 & 16).

The Laba-Buulgen Lower-Middle Palaeozoic oceanic accretionary complex (including the subordinate Chugush and Kassar successions; Figure 16, Lower-Middle Palaeozoic basite-ultrabasite-thonalite metamorphic complexes) represents the southernmost strip of the mafic series along the southern edge of the Crystalline Core Zone of the Great Caucasus. It extends for about ~300 km, is 10–20 km wide and has a thickness varying from 2500 m to 3500 m. This complex is the largest pre-Upper Palaeozoic oceanic unit in the Great Caucasus. It is composed mainly of diverse tectonic slices of metamorphosed palaeo-oceanic lithosphere that includes mantle residuals, ultrabasic and basic meta-cumulates, gabbro-amphibolites, garnet-amphibolites, amphibolites, various mica schists, paragneisses and marbles, associated with tonalite-gneisses, diorite-gneisses, plagiogneisses, etc. The whole complex experienced regional metamorphism under high- to low-pressure (7.0–2.5 kb) epidote-amphibolite to amphibolite facies conditions. Two main types of metavolcanic series are distinguished: (a) a series of high-Ti basalts, and (b) a differentiated

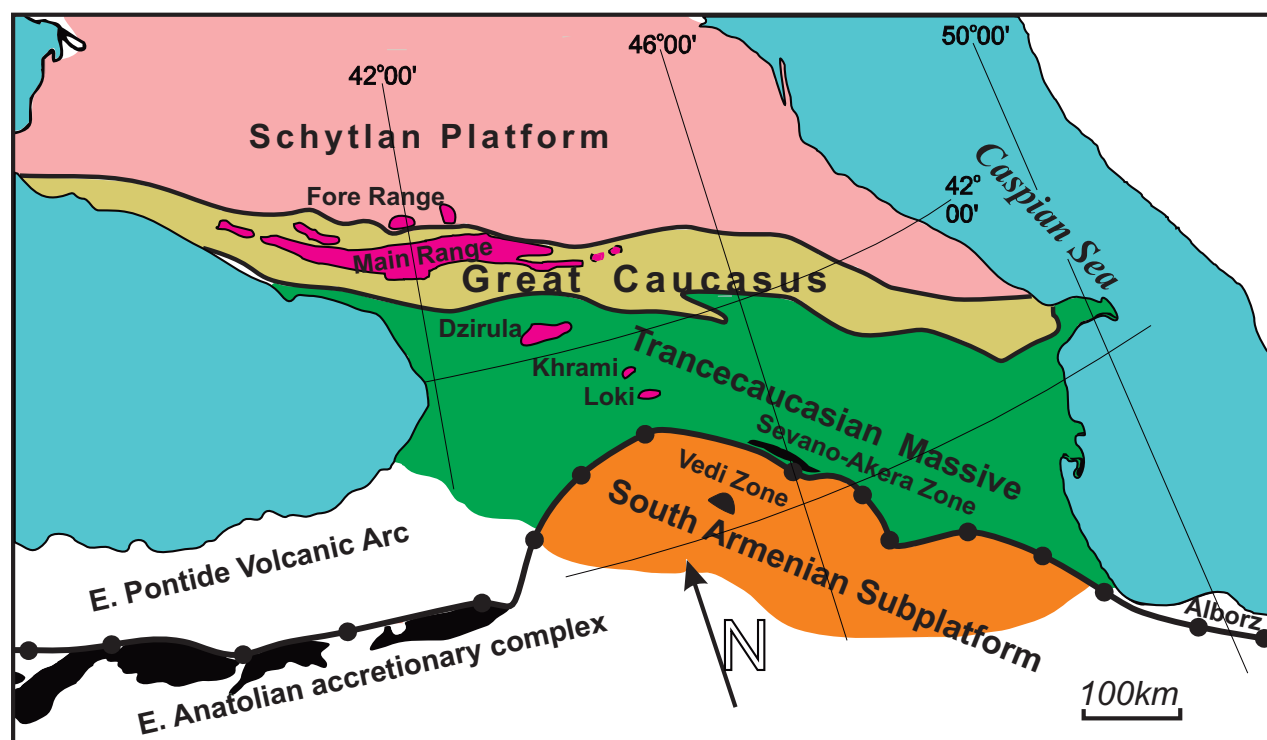
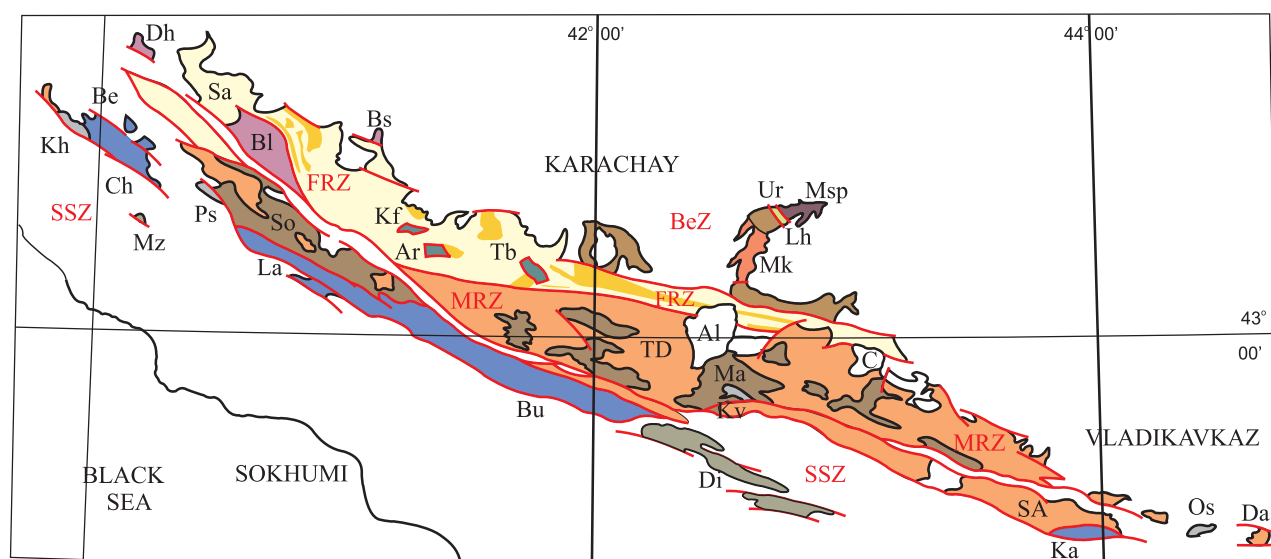













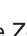


Figure 15. Tectonic scheme of the Caucasus.



- | | |
|---|---|
|  Devonian-Triassic deposits of the Dizi series (Di) and Triassic of the Mzimta |  Upper Palaeozoic deposits: Khuko (Kh), Pseashko (Ps), Kvishi (Kv), and Oseti (Os) |
|  Lower-Middle Palaeozoic basite-ultrabasite-tonalite metamorphic complexes: Belaia (Be), Chugush (Ch), Laba (La), Buulgen (Bu), and Kassar (Ka); |  Lower-Middle Palaeozoic metapelite-gneiss-migmatite Macera etc complexes (Mc) |
|  Upper Palaeozoic (Variscan-Vs) granitic complexes |  Palaeozoic-Triassic volcanic and sedimentary complexes |
|  Lower-Middle Palaeozoic basite-ultrabasite metamorphic complexes: Blib (Bl), Dakhov (Dh), Sahrai (Sa), and Beskes (Bs). |  Lower-Middle Palaeozoic ophiolites allochtones: Kjafar (Kf), Arkhiz (Ar), Teberda (Tb), Bechasin zone (BeZ) |
|  Lower-Middle Palaeozoic metamorphic Chegem etc complexes |  Lower-Middle Palaeozoic deposits: Urlesh (Ur), Lahran (Ln) etc suits |
|  Upper Palaeozoic Malka (Mk) granites |  Malka serpentinites (Msp) |
|  Middle Palaeozoic volcanic complexes: Urup etc. formations |  faults, thrusts |

BeZ Bechasin zone **FRZ** Fore Range Zone **MRZ** Main Range Zone **SSZ** Southern Slope Zone

Tectonic megaslices: Sofia (So), Teberda-Digor (TD), Shkhara-Adaihoh (SA). Extinct volcanoes: Elbrus (El), Chegem (C)

Figure 16. Geological sketch of the Hercynides of the Great Caucasus.

series of low-Ti basalt-andesite-dacite-rhyolite (Adamia *et al.* 2004; Zakariadze *et al.* 2009). The high-Ti basalts ($\text{TiO}_2 = 1.75\text{--}3.47$ wt%) correspond to olivine-nepheline and olivine-hyperstene-normative tholeiitic ($\text{K}_2\text{O} = 0.34 \pm 0.10$ wt%) and subalkaline ($\text{K}_2\text{O} = 0.93 \pm 0.42\%$) types. Tholeiites show a weak depletion in LREE [$(\text{La}/\text{Sm})_n = 0.99 \pm 0.03$; $(\text{La}/\text{Yb})_n = 0.94 \pm 0.10$; $(\text{Sm}/\text{Yb})_n = 0.95 \pm 0.09$], and subalkaline varieties a moderate enrichment in LREE [$(\text{La}/\text{Sm})_n = 2.18 \pm 0.98$; $(\text{La}/\text{Yb})_n = 3.52 \pm 2.80$; $(\text{Sm}/\text{Yb})_n = 1.49 \pm 0.87$]. These rock groups are confidently

attributed to N-T-MORB type series. Basalts of the low-Ti basalt-andesite-dacite-rhyolite series correspond to low-Ti ($\text{TiO}_2 = 0.46\text{--}1.09$ wt %), fractionated ($\text{Mg}^\# = 0.72\text{--}0.45$), Ol-Hy-normative compositions with widely variation in Al content ($\text{Al}_2\text{O}_3 = 15.43\text{--}21.04\%$). Among these basalts are also those displaying rather flat REE patterns [$(\text{La}/\text{Sm})_n = 0.93 \pm 0.22$; $(\text{La}/\text{Yb})_n = 0.74 \pm 0.03$; $(\text{Sm}/\text{Yb})_n = 0.82 \pm 0.16$; $(\text{Tb}/\text{Yb})_n = 0.83 \pm 0.03$] and also those relatively more enriched with LREE [$(\text{La}/\text{Sm})_n = 2.30 \pm 0.68$, $(\text{La}/\text{Yb})_n = 3.18 \pm 1.83$; $(\text{Sm}/\text{Yb})_n = 1.33 \pm 0.42$]. These are

identified as SSZ type, transitional from tholeiitic to calc-alkaline. The proportions of the metavolcanic series and metasediments vary in different parts of the complex. For example in the Buulgen sections, high-Ti basalts and metasediments dominate whereas in the Laba sections the differentiated volcanic series are prevalent. Note that Th/REE ratios in all basalts of the Laba-Buulgen Complex are slightly higher than those from basalts of oceanic spreading zones (Th/La= 0.20 ± 0.08 ; Th/Sm= 0.38 ± 0.05 ; Th/Yb= 0.34 ± 0.03), and that is considered as a SSZ-type feature for the entire complex. Fossils of crinoids, corals, cyanobacteria and foraminifera found in marbles indicate an Early–Middle Palaeozoic age for these rocks. Magmatic zircons from orthogneisses show a time interval of 380–312 Ma, which also indicates a middle Palaeozoic age for the metavolcanic and sedimentary series (Adamia *et al.* 2011; Somin 2007a). The age of regional metamorphism is accepted as Late Palaeozoic. As a whole the Laba-Buulgen Complex is interpreted as a heterogeneous Palaeozoic oceanic accretionary complex of immature island arc-marginal sea type, which was accreted to the southern edge of an island arc of the Great Caucasus and was metamorphosed in the Late Palaeozoic.

In the Fore Range tectonic zone of the Great Caucasus, Hercynian tectonic events are reported, characterized by accretion and deformation of thick Middle Palaeozoic successions and the formation of Upper Palaeozoic molasses. Upper Palaeozoic (Hercynian) granites are totally absent here. The geological sketches of thrust-sheet structures of the Fore Range Zone of the Great Caucasus are presented in Figures 16 and 17. The oceanic Palaeozoic successions are displayed here in the Blib, Urup, Marukh and Atsgara tectonic sheets.

From these the Blib metamorphic mafic complex (assumed to be allochthonous) occurs at the visible base of the Fore Range Zone (Lower–Middle Palaeozoic basite-ultrabasic metamorphic complexes on Figure 16). The 2000-metres-thick lower part of the complex is composed mainly of mafic rocks: garnet, epidote and albite amphibolites of primarily volcanic origin. Amphibole gneisses, garnet-two mica schists and plagiogneisses are also represented. The Upper, basically metasedimentary part of the complex (1500

m), is made up of garnet-mica- and quartz-albite-chlorite-epidote-muscovite schists, garnet-quartz-muscovite schists and amphibolites. All along the section there are lenses of serpentized ultrabasics, associated with amphibolites and eclogites. Metavolcanics and metasediments are associated with masses of meta-plagiogranites, tonalite-gneisses, granodiorite-gneisses and plagiogneisses. All metamorphic rocks of the Blib Complex underwent LT/HP metamorphism. The highest pressures are established for eclogite bodies ($T= 650^{\circ}\text{C}$, $P= 14\text{--}16$ kb; Shengelia *et al.* 1991; Perchuk 2003). Metamorphism at shallower depth is represented by garnet amphibolites with patches of kyanite-garnet schists, phengite-amphibole orthogneisses and meta-plagiogranites with phengite mica ($T= 550^{\circ}\text{C}$, $P= 8\text{--}9$ kb; Korikovskiy *et al.* 2004). The protolith composition of the metabasics corresponds to SSZ-type basalts, for which increased Th/REE ratios (Th/La= 0.48 ± 0.10 ; Th/Sm= 0.81 ± 0.20 ; Th/Yb= 0.65 ± 0.21) and negative Nb geochemical anomalies are characteristic. U-Pb dating of the protolith of the magmatic rocks (gabbro-amphibolite and apogranitic orthogneisses) of the Blib complex provides an interval of 400–355 Ma (Somin & Lavrishev 2005; Somin 2007a; Somin *et al.* 2007). The age range for HP metamorphism is established as 360–320 Ma, while for the eclogites the age range is 322–305 Ma (K-Ar, Ar-Ar, Rb-Sr, Lu-Hf; Somin 1991; Perchuk & Phillipot 1997; Phillipot *et al.* 2001; Perchuk 2003).

Thus, the crystalline base of the Fore Range Zone of the Great Caucasus is a heterogeneous complex of Devonian SSZ-type (Perchuk 2003; Korikovskiy *et al.* 2004; Adamia *et al.* 2011) magmatic series, formed in an ensimatic setting.

The mafic crystalline base of the Fore Range Zone is overlain by the volcanic Urup supra-subduction zone type complex (> 2 km), closely associated with a terrigenous-carbonate series of Silurian–Devonian–Early Carboniferous age (Figures 16 & 17; Middle Palaeozoic volcanic complexes, e.g., Urup formation). The contacts of the complex with surrounding rocks are basically tectonic. Only above it is progressively replaced by terrigenous-carbonate deposits of Late Devonian–Early Carboniferous age. The biostratigraphically substantiated age interval of the complex as a whole extends from the Lower

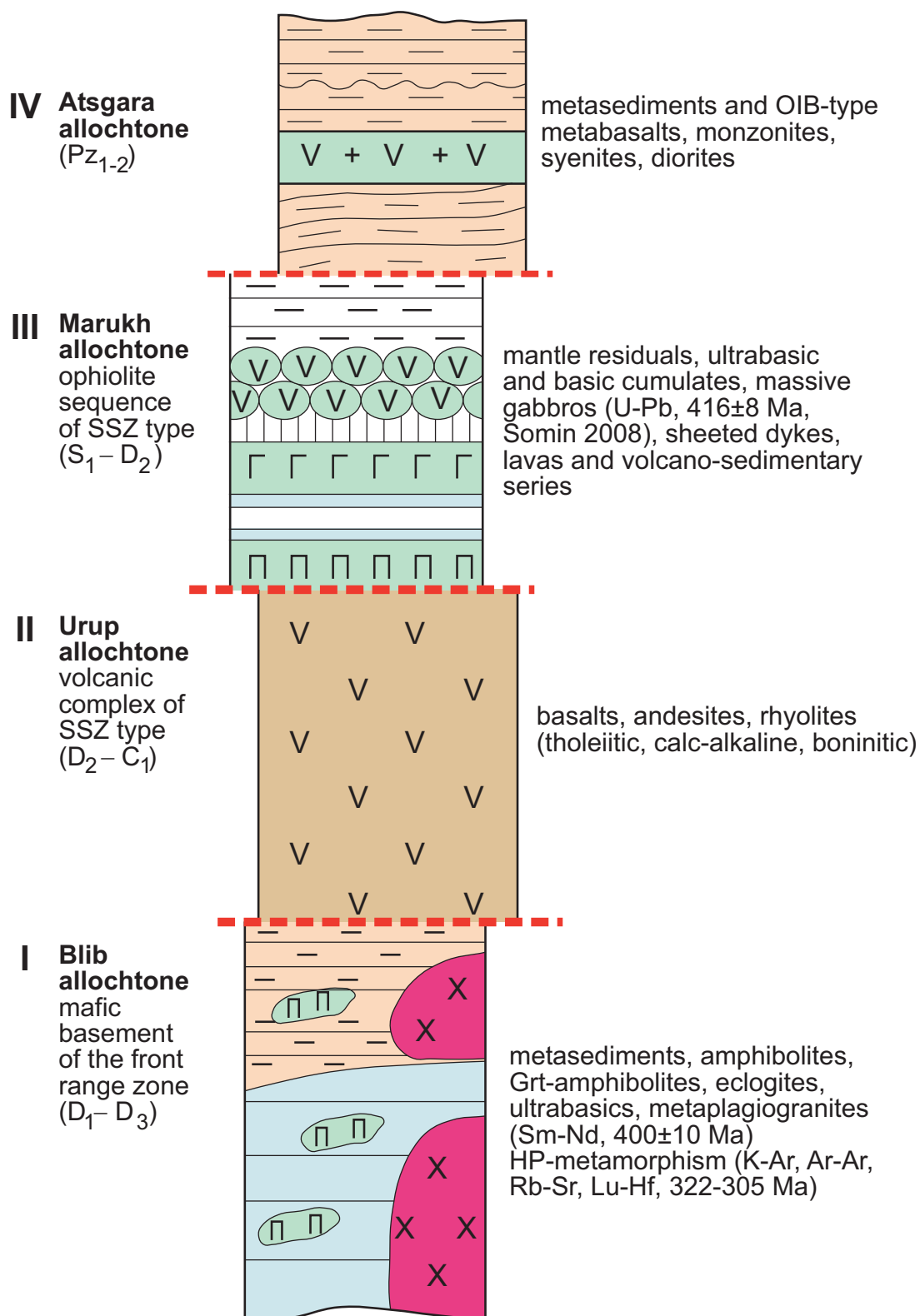


Figure 17. The Hercynian fault-thrust structure of the Fore Range Zone of the Great Caucasus.

Silurian to the Lower Carboniferous (Shavishvili 1983, 1988; Somin 2007a). The volcanics, comprising a continuous compositional range from basalts to rhyolites, have experienced greenschist facies regional metamorphism, but their primary composition is well preserved. Their major element compositions show them to be an SSZ-type series transitional from tholeiitic to calc-alkaline. Restricted amounts of alkali basaltic and boninitic flows are also present.

The overlying allochthonous unit in the Fore Range Zone is the overthrust Marukh ophiolite complex, with a total thickness of 2000 m (Grekov *et al.* 1974; Adamia & Shavishvili 1982; Adamia 1989; Khain 1984; Adamia *et al.* 2004; Somin 2007a, b, 2009; Adamia *et al.* 2011; Figures 16 & 17, Lower–Middle Palaeozoic ophiolite allochthones). The complex is dismembered and sliced, but provides a complete ophiolite sequence with mantle residuals, ultrabasic-basic cumulates, dyke swarms and lava flows, and is associated with terrigenous, carbonate and volcanoclastic sediments. In the mantle residuals serpentinized harzburgites predominate. Gradual transitions are observed between the cumulate and dyke series and the lava flows. The prominent feature of the Marukh ophiolite complex is a consistent display of magmatic formations of intermediate (andesitic) composition, gabbro-diorites and diorites in the cumulate series, diorite bodies in dyke swarms, and low-Ti basalts ($\text{TiO}_2 < 1 \text{ wt}\%$), basaltic andesites and andesites in lava flows. The latter occur in the volcanic and volcanic-sedimentary successions at the top of the ophiolite sequence. All rocks in the complex experienced greenschist facies regional metamorphism. The complex is overlain by Hercynian molasse of Bashkirian age. In the part of the pre-Caucasus adjoining the Fore Range Zone to the north, there is a continuous formation of ophiolitic olistostroms from Upper Silurian to Lower Carboniferous. The Devonian oceanic lithosphere is confirmed by the discovery of corals in the volcano-sedimentary series (Grekov *et al.* 1974) and by zircon dating (SHRIMP) from cumulate gabbros ($416 \pm 8 \text{ Ma}$; Somin 2007a). The problem of the root zone of the ophiolite allochthons so far is debatable. Some authors place it in the extreme south of the Crystalline Core Zone (Laba-Buulgen metabasic complex) thrust over the southern boundary of the Fore Range Zone of the Great Caucasus.

At the top of the sequence in the pre-Upper Palaeozoic structure in the Fore Range Zone of the Great Caucasus, is the Atsgara allochthonous unit (500–700 metres thick; Figures 16 & 17, Lower–Middle Palaeozoic ophiolite allochthons). It consists of a series of tectonic sheets of metamorphic rocks, differing from each other in formational types and P/T conditions of metamorphism, comprising mainly metasediments (metapelites, greywackes, parashists) and strongly subordinate metabasics (amphibolites and amphibole schists). The protoliths of the latter were alkaline olivine basalts of within-plate type. The metamorphic conditions of the whole complex range from amphibolite to greenschist facies. Metamorphics associated with intrusive rocks are represented by the diorite-quartz-diorite-tonalite-trondhjemite series and K-feldspar-bearing gabbro-monzogabbro-monzonite-syenite. Reliable geochronological data from the Atsgara Unit are very scarce. The magmatic series is probably Early Palaeozoic, while the age of regional metamorphism of the complex is probably Middle Palaeozoic (D_1 – D_3) (Shavishvili *et al.* 1989; Somin 1991, 2007a, b).

Comparative Features of pre-Hercynian Palaeo-oceanic Zones of the BCO and Great Caucasus and Final Remarks

1. Middle Palaeozoic oceanic rock series within the Eastern Mediterranean Hercynides (BCO, Great Caucasus) described in this paper reflect some features of the evolution of the European continental margin, predating extensive collisional events in the Late Palaeozoic. Undoubtedly the established relationships require further study and more detailed data; but even now it is possible to outline some main features of the Middle Palaeozoic oceanic complexes.
2. Within the BCO similar oceanic complexes, but of different ages Neoproterozoic–Lower Cambrian, and Middle Palaeozoic (Devonian), are distinguished. Both occur along the Thracian oceanic suture. The history of the Thracian suture, thus, demands more detailed study.
3. In the Great Caucasus Proterozoic–Cambrian oceanic crust has not been recognized. The Palaeozoic ocean is believed to have been south

of the Great Caucasus Hercynides (Laba-Buulgen Complex, Figure 16); it was probably derived from the Proterozoic–Early Palaeozoic ocean separating Baltica and Gondwana, which was completely subducted (Adamia *et al.* 2011). Note, however, that unlike BCO the Middle Palaeozoic oceanic complexes of the Great Caucasus show exclusively SSZ type features.

4. Areas of the Eastern Mediterranean Hercynides situated south of the putative Early–Middle Palaeozoic oceanic suture zones of the Balkanides and the Great Caucasus carry a clear record of Cadomian orogenic events (Chen *et al.* 2002; Kounov 2002; Zakariadze *et al.* 2002,

2007; Arkadaskiy *et al.* 2003; Yiğitbaş *et al.* 2004; Carrigan *et al.* 2005; Liati 2005; Ustaömer *et al.* 2005; Kounov *et al.* 2006). They can be conditionally united in a peri-Gondwanan Thracian-Pontide-Transcaucasian Composite Terrane, which collided with the European margin in the Late Palaeozoic.

Acknowledgments

We are grateful to Yuri Kostitsin, Alexander Kotov and Dmitry Zhuravlev for their critical comments during manuscript preparation. This study was funded by a RFFI (Russian Foundation of Fundamental Research) grant 08-05-00-503.

References

- ADAMIA, SH. 1989. Paleotethys, Mesotethys, Neotethys – various oceans or different stages of Tethys development. *Proceedings of Geological Institute of Academy of Sciences of Georgia* **99**, 18–49 [in Russian].
- ADAMIA, SH., ASANIDZE, B., CHKHOTUA, T., KEKELIA, M., SHAVISHVILI, I., TSIMAKURIDZE, G. & ZAKARIADZE, G. 2004. Fragments of Palaeo-Tethian terranes in the crystalline core of the Great Caucasus. In: CHATZIPETROS A.A. & PAVLIDES S.B. (eds), *Proceedings of the 5th International Symposium on Eastern Mediterranean Geology*. Thessaloniki, Greece, 233–236.
- ADAMIA, SH., BELOV, A., KEKELIA, M. & SHAVISHVILI, I. 1987. Palaeozoic tectonic development of the Caucasus and Turkey (Geotravers G). In: FLÜGEL, H.W., SASSI, F.P. & GRECU, P. (eds), *Pre-Variscan and Variscan Events in the Alpine-Mediterranean Mountain Belts*. Bratislava, 23–50, Alfa Publishers.
- ADAMIA, SH., CHKHOTUA, T., KEKELIA, M., LORDKIPANIDZE, M., SHAVISHVILI, I. & ZAKARIADZE, G. 1981. Tectonics of the Caucasus and adjoining regions: implications for the evolution of the Tethys ocean. *Journal of Structural Geology* **3**, 437–447.
- ADAMIA, SH. & SHAVISHVILI, I. 1982. Root zone of the ophiolite nappes of the Western Caucasus. *Doclady of Academy of Sciences of the USSR*, volume **267**, 1424–1425 [in Russian].
- ADAMIA, SH., ZAKARIADZE, G., CHKHOTUA, T., SADRADZE, N., TSERETELI, N., CHABUKIANI, A. & GVENTSADZE, A. 2011. The Caucasus: an example of Late Cenozoic continent-continent collision structure. *Turkish Journal of Earth Sciences* **20**, 489–544.
- ARISKIN, A.A. 1999. Phase equilibria modeling in igneous petrology: use of COMAGMAT model for simulating fractionation of ferro-basaltic magmas and the genesis of high-alumina basalt. *Journal of Volcanology and Geothermal Research* **90**, 115–162.
- ARISKIN, A.A. & BARMINA, G.S. 2000. *Modeling Phase Equilibria During the Crystallization of Basaltic Magma*. Nauka, Moscow [in Russian].
- ARISKIN, A.A. & BARMINA, G.S. 2004. COMAGMAT: development of a magma crystallization model and its petrological applications. *Geochemistry International* **42**, Supplement **1**, 1–157.
- ARKADASKIY, S., BÖHM, C., HEAMAN, L., CHERNEV, Z. & STANCHEVA, E. 2003. Remnants of Neoproterozoic oceanic crust in the Central Rhodope metamorphic complex. Bulgaria. *Abstracts, The Geological Society, America, Vancouver Annual Meeting*, 3–62.
- BLACK, L.P., KAMO, S.L., ALLEN, C.M., ALEINIKOFF, J.N., DAVIS, D.W., KORSCH, R.J. & FOUODOULIS, C. 2003. TEMORA 1: a new zircon standard for U-Pb geochronology. *Chemical Geology* **200**, 155–170.
- CARRIGAN, CH.W., MUKASA, S.B., HAYDOUTOV, I. & KOLCHEVA, K. 2005. Age of Variscan magmatism from the Balkan sector of the orogen, central Bulgaria. *Lithos* **82**, 125–147.
- CHEN, F., SIEBEL, W., SATIR, M., TERZİOĞLU, M.N. & SAKA, K. 2002. Geochronology of the Karadere basement (NW Turkey) and implications for the geological evolution of the İstanbul zone. *International Journal of Earth Sciences* **91**, 469–481.
- CHRISTIE, D.M., CARMICHAEL, I.S.E. & LANGMUIR, C.H. 1986. Oxidation states of mid-ocean ridge basalt glass. *Earth and Planetary Science Letters* **79**, 397–411.
- CROWLEY, Q.G., FLOYD, P.A., WINCHESTER, J.A., FRANKE, W. & HOLLAND, J.G. 2000. Early Palaeozoic rift-related magmatism in Variscan Europe: fragmentation of the Armorican Terrane assemblage. *Terra Nova* **12**, 171–180.
- DAL PIAZ, G.V., BISTACCHI, A. & MASSIRONI, M. 2003. Geological outline of the Alps. *Episodes* **26**, 175–180.

- DANYUSHEVSKY, L.V. 2001. The effect of small amounts of H₂O on crystallization of mid-ocean ridge and backarc basin magmas. *Journal of Volcanology and Geothermal Research* **110**, 265–280.
- DANYUSHEVSKY, L.V., PERFIT, M.R., EGGINS, S.M. & FALLOON, T.J. 2003. Crustal origin for coupled ‘ultra-depleted’ and ‘plagioclase’ signatures in MORB olivine-hosted melt inclusions: evidence from the Siqueiros Transform Fault, East Pacific Rise. *Contributions to Mineralogy and Petrology* **144**, 619–637.
- DANYUSHEVSKY, L.V., LESLIE, R.A.J., CRAWFORD, A.J. & DURANCE, P. 2004. Melt inclusions in primitive olivine phenocrysts: the role of localized reaction processes in the origin of anomalous compositions. *Journal of Petrology* **45**, 2531–2553.
- GOLDSTEIN, S.L., O’NIONS, R.K. & HAMILTON, P.J. 1984. A Sm-Nd isotopic study of atmospheric dusts and particulates from major river systems. *Earth and Planetary Science Letters* **70**, 221–236.
- GOVINDARAJU, K. 1994. *Compilation of Working Values and Sample Description for 383 Geostandarts*. Geostandards Newsletters, special issue **18**, 1–158.
- GREKOV, I., KROPACHEV, S., MOMOT, S. & KOREN, T. 1974. Marukh Palaeozoic nappe of the Northern Caucasus. *Sovetskaia Geologia* **2**, 77–85 [in Russian].
- HAYDOUTOV, I. 1989. Precambrian ophiolites, Cambrian island arc, and Variscan suture in the South Carpathian-Balkan region. *Geology* **17**, 905–908.
- HAYDOUTOV, I. 1991. *Origin and Evolution of the Precambrian Balkan-Carpathian Ophiolite Segment*. Bulgarian Academy of Sciences, Sofia, **179** [in Bulgarian with English summary].
- HAYDOUTOV, I., DAIEVA, L. & KOLCHEVA, K. 1993. Ophiolite blocks in the Diabase-Phyllitoid Complex from SW Bulgaria. *Reviews of Bulgarian Geological Society LIV* **3**, 60–70.
- HAYDOUTOV, I., GOCHEV, P., KOZHOUKHAROV, D. & YANEV, S. 1996–1997. Terranes in the Balkan area. In: PAPANIKOLAOU (eds), *IGCP Project No. 276, Palaeozoic Geodynamic Domains and Their Alpidic Evolution in the Tethys; Terrane Maps and Terrane Descriptions*, 479–494.
- HAYDOUTOV, I. & YANEV, S. 1997. The Protomoesian microcontinent of the Balkan Peninsula – a peri-Gonwanaland piece. *Tectonophysics* **272**, 303–313.
- HOFMANN, A.W. 1997. Mantle geochemistry: the message from oceanic volcanism. *Nature* **385**, 219–229.
- KALVODA, J., BABEK, O., FATKA, O., LEICHMANN, J., MELICHAR, R., NEHYBA, S. & SPACEK, P. 2008. Brunovistulian terrane (Bohemian Massif, Central Europe) from late Proterozoic to late Palaeozoic: a review. *International Journal of Earth Sciences* **97**, 497–518.
- KARAMATA, S. & KRSTIĆ, B. 1996. Terranes of Serbia and neighboring areas. In: KNEZEVIC, V. & KRSTIC, B. (eds), *Terranes of Serbia*. Faculty of Mining and Geology, University of Belgrade Committee for Geodynamics of the Serbian Academy of Sciences and Art, 25–40.
- KARAMATA, S., KRSTIĆ, B., DIMITRIJEVIĆ, M., DIMITRIJEVIĆ, V., KNEEVIĆ, R., STOJANOV, J. & FILIPOVIĆ 1996–1997. Terranes between the Moesian plate and the Adriatic Sea. In: PAPANIKOLAOU (eds), *IGCP Project No. 276, Palaeozoic Geodynamic Domains and Their Alpidic Evolution in the Tethys; Terrane Maps and Terrane Descriptions*, 429–477.
- KEBEDE, T., KLÖTZLI, U., KOSLER, J. & SKIÖLD, T. 2005. Understanding the pre-Variscan and Variscan basement components of the central Tauern Window, Eastern Alps (Austria): constraints from single zircon U–Pb geochronology. *International Journal of Earth Sciences* **94**, 336–353.
- KEPPIE, J.D., NANCE, R.D., MURPHY, J.B. & DOSTAL, J. 2003. Tethyan, Mediterranean, and Pacific analogs for the Neoproterozoic–Palaeozoic birth and development of peri-Gondwanan terranes and their transfer to Laurentia and Laurussia. *Tectonophysics* **365**, 195–219.
- KHAIN, E.B. 1984. *Ophiolites and Hercynian Tectonic Sheet Structure of the Fore Range of the Northern Caucasus*. Moscow, Nauka, **94** [in Russian].
- KORIKOVSKY, S.P., SOMIN, M.L. & KORSKOV, S.G. 2004. Symplectitic high-pressure garnet-margarite-muscovite-clinozoisite amphibolites of Dakhov salient (northern Caucasus): origin and composition of reactional textures. *Reports of Academy of Sciences (RAS)* **397**, 650–654 [in Russian].
- KOUNOV, A. 2002. *Termotectonic Evolution of Kraishite, Western Bulgaria*. PhD Thesis, Swiss Federal Institute of Technology Zürich, Natural Sciences, **219**.
- KOUNOV, A., SEWARD, D., BERNOULLI, D., BURG, J.-P. & IVANOV, Z. 2006. Evidence for Cadomian ophiolite and island arc complex in SW Bulgaria. *Proceedings of International Symposium Mesozoic Ophiolite Belts of Northern Part of Balkan Peninsula, Belgrade-Banja Luka, May 31–June 6*, 67–69.
- KRÄUTNER, H.G. & KRSTIĆ, B. 2003. *Geological Map of the Carpatho-Balkanides Between Mehadia, Oravita, Niš and Sofia*. Geoinstitute Belgrade.
- LIATI, A. 2005. Identification of repeated Alpine (ultra) high-pressure metamorphic events by U–Pb SHRIMP geochronology and REE geochemistry of zircon: the Rhodope zone of Northern Greece. *Contributions to Mineralogy and Petrology* **150**, 608–630.
- LUDWIG, K.R. 1999. *User’s Manual for Isoplot/Ex, Version 2.10, A Geochronological Toolkit for Microsoft Excel*. Berkeley Geochronology Center, Special Publication **1a**, 2455 Ridge Road, Berkeley CA 94709, USA.
- LUDWIG, K.R. 2000. *SQUID 1.00, A User’s Manual*. Berkeley Geochronology Center, Special Publication **2**, 2455 Ridge Road, Berkeley, CA 94709, USA.
- MĂRUNTU, M. 1984. The inner structure and petrology of the Tisovita-Iuti ophiolite complex. *Studii și Cercetări de Geologie Geofizică Geografie, Series Geologie* **29**, 44–54 [in Romanian].
- MATTE, P. 1991. Accretionary history and crustal evolution of the Variscan belt in Western Europe. *Tectonophysics* **196**, 309–337.

- NATLAND, J.H. & DICK, H. 2001. Formation of lower ocean crust and the crystallization of gabbroic cumulates at a very slowly spreading ridge. *Journal of Volcanology and Geothermal Research* **110**, 191–233.
- NIELSEN, R.L., CRUM, J., BOURGEOIS, R., HASCALL, K., FORSYTHE, L.M., FISK, M.R. & CHRISTIE, D.M. 1995. Melt inclusions in high-An plagioclase from the Gorda Ridge: an example of the local diversity of MORB parent magmas. *Contributions to Mineralogy and Petrology* **122**, 34–50.
- PERCHUK, A.L. 2003. *Petrology and Mineral Chronometry of the Crustal Eclogites*. PhD Thesis, IGEM RAS, **48**. Moscow, Russia.
- PERCHUK, A. & PHILLIPPOT, P. 1997. Rapid cooling and exhumation of eclogitic rocks from the Great Caucasus, Russia. *Journal of Metamorphic Geology* **15**, 299–310.
- PHARAOH, T.C. 1999. Palaeozoic terranes and their lithospheric boundaries within the Trans-European Suture Zone (TESZ): a review. *Tectonophysics* **314**, 17–41.
- PHILLIPPOT, P., Blichert-Toft, J., PERCHUK, A., COSTA, S. & GERASIMOV, V. 2001. Lu-Hf and Ar-Ar chronometry supports extreme rate of subduction zone metamorphism deduced from geospeedometry. *Tectonophysics* **342**, 23–38.
- PIN, C. 1990. Variscan oceans: ages, origins and geodynamic implications inferred from geochemical and radiometric data. *Tectonophysics* **177**, 215–227.
- RICHARD, P., SHIMIZU, N. & ALLEGRE, C.J. 1976. $^{143}\text{Nd}/^{146}\text{Nd}$ a natural tracer: an application to oceanic basalts. *Earth and Planetary Scientific Letters* **31**, 269–278.
- SAVOV, I., RYAN, J., HAYDOUTOU, I. & SCHIJE, J. 2001. Late Precambrian Balkan-Carpathian ophiolite – a slice of the Pan-African ocean crust?: geochemical and tectonic insights from the Tcherni Vrach and Deli Jovan Massif, Bulgaria and Serbia. *Journal of Volcanology and Geothermal Research* **110**, 299–318.
- SCHULZ, B., BOMBACH, K., PAWLIG, S. & BRÄTZ, H. 2004. Neoproterozoic to Early-Palaeozoic magmatic evolution in the Gondwana-derived Austroalpine basement to the south of the Tauern Window (Eastern Alps). *International Journal of Earth Sciences* **93**, 824–843.
- SHAVISHVILI, I.D. 1983. Variscan volcanism in the Caucasus. In: SASSI & SZEDERKNEYI (eds), *IGCP No. 5, Newsletter* **5**, 169–179.
- SHAVISHVILI, I.D. 1988. Boninites and high-magnesian basalts of the Fore Range of the Great Caucasus. *Abstracts, 'Geology of Oceans and Seas', 8th All-union School of Marine Geology* **2**, 159–160. Moscow.
- SHAVISHVILI, I.D., ABESADZE, M.B. & CHKHOTUA, T.G. 1989. Features of composition and condition of formation of rocks of Atsgara tectonic sheet of the Fore Range of the Great Caucasus. *Proceedings, 'Geodynamics of the Caucasus'*, Nauka, Moscow, 73–81 [in Russian].
- SHENGELIA, D.M., KORIKOVSKY, S.P., CHICHINADZE, G.L., MGALOBILSHVILI, I.Z., KAKHADZE, R.G., POPORADZE, N.G., SOMIN, M.L., POTAPENKO, Y.N., KETSKHOVELI, D.H., OKROSTVARIDZE, A.B., SHENGELIA, M.D., TSUTSUNAVA, T.N., GERASIMOV, V.Y. & PERCHUK, A.L. 1991. *Petrology of Metamorphic Complexes of the Great Caucasus*. Nauka, Moscow [in Russian].
- SOMIN, M.L. 1991. Geological characteristics of the metamorphic complexes of the Great Caucasus. In: KORIKOVSKY, S.P. (ed), *Petrology of Metamorphic Complexes of the Great Caucasus*, Nauka, Moscow, 8–43.
- SOMIN, M.L. 2007a. *Structural Position and Geodynamic Conditions of Formation of Metamorphic Complexes of the Great Caucasus and Cuba*. PhD Thesis, Shmidt Institute of Earth Physics, RAN, Moscow.
- SOMIN, M.L. 2007b. Main features of structures of the pre-Alpine basement of the Great Caucasus. In: LEONOV, Y.G. (ed), *Rock Complexes and Geodynamics of the Main Stages of Evolution of the Great Caucasus*. Moscow, GEOS, 10–52 [in Russian].
- SOMIN, M.L. 2009. Geology of crystalline basement of the Greater Caucasus: new data. *Abstracts, 2nd International Symposium on the Geology of the Black Sea Region, 5–9 October 2009, Ankara, Turkey*, 186–187.
- SOMIN, M.L. & LAVRISCHEV, V.A. 2005. The combined complexes in structure of the Fore Range of the Great Caucasus. *Reports of RAS* **401**, 370–372.
- SOMIN, M.L., LEVCHENKO, O., KOTOV, A., MAKEEV, A., KOMAROV, A., LAVRISCHEV, V. & LEBEDEV, V. 2007. The Palaeozoic age of high-pressure metamorphic rocks in the Dakhov salient, Northwestern Caucasus: results of U-Pb geochronological investigations. *Doklady on Earth Sciences* **416**, 1018–1021.
- SPEAR, F.S. 1995. Metamorphic phase equilibria and pressure-temperature-time pass. In: *The Metamorphism of Mafic Rocks*, 393–446. Mineralogical Society of America, Monograph.
- SUN, S.S. & McDONOUGH, W.F. 1989. Chemical and isotopic systematics of oceanic basalts: implications for mantle composition and process. *Geological Society Special Publications* **42**, 313–345.
- TERZIĆ-PERKOVIĆ, M. 1960. Petrološko proučavanje gabrova masiva Deli Jovana. *Geološki anali Balkanskog poluostrva* **XXVII**, 327–403 [in Serbian].
- USTAÖMER, P.A., MUNDIL, R. & RENNE, P.R. 2005. U/Pb and Pb/Pb zircon ages for arc-related intrusions of the Bolu Massif (W Pontides, NW Turkey): evidence for Late Precambrian (Cadomian) age. *Terra Nova* **17**, 215–223.
- VON RAUMER, J.F., STAMPFLI, G.M., BOREL, G. & BUSSY, F. 2002. Organization of pre-Variscan basement areas at the north-Gondwanan margin. *International Journal of Earth Sciences* **91**, 35–52.
- VON RAUMER, J.F., STAMPFLI, G.M. & BUSSY, F. 2003. Gondwana-derived microcontinents – the constituents of the Variscan and Alpine collisional orogens. *Tectonophysics* **365**, 7–22.
- VON QUADT, A.V.A., PEYTCHEVA, I. & HAYDOUTOV, I. 1998. U-Pb zircon dating of Tcherny Vrach metagabbro, the West Balkan, Bulgaria. *Comptes rendus de l'Academie Bulgare des Sciences, Sofia* **51**, 86–89.
- WETHERILL, G.W. 1956. Discordant uranium-lead ages. *Transactions-American Geophysical Union* **37**, 320–326.
- WILLIAMS, I.S. 1998. U-Th-Pb geochronology by ion microprobe. In: MCKIBBEN, M.A., SHANKS III, W.C. & RIDLEY, W.I. (eds), *Applications of Microanalytical Techniques To Understanding Mineralizing Processes, Reviews in Economic Geology* **7**, 1–35.

- YİĞİTBAŞ, E., KERRICH, R., YILMAZ, Y., ELMAS, A. & XIE, Q. 2004. Characteristics and geochemistry of Precambrian ophiolites and related volcanics from the İstanbul-Zonguldak Unit, Northwestern Anatolia, Turkey: following the missing chain of the Precambrian South European suture zone to the east. *Precambrian Research* **132**, 179–206.
- YANEV, S. 2000. Palaeozoic terranes of the Balkan Peninsula in the framework of Pangea assembly. *Palaeogeography, Palaeoclimatology, Palaeoecology* **161**, 151–177.
- ZAKARIADZE, G.S., ADAMIA, SH., CHKHOTUA, T., KEKELIA, M., SHAVISHVILI, I. & TSIMAKURIDZE, G. 2002. *Geodynamic Evolution of the Pre-Alpine Basement of Georgia (Transcaucasus)*. *Geologica Carpathica* **53**, Special Issue 3-4.
- ZAKARIADZE, G.S., CHKHOTUA, T., ADAMIA, SH., SHAVISHVILI, I. & KUTELIA, Z. 2009. Relics of Prototethyan and Palaeotethyan Oceanic Lithosphere in the Caucasus. *Abstracts, 2nd International Symposium on the Geology of the Black Sea Region, 5–9 October 2009, Ankara, Turkey*, 238–239.
- ZAKARIADZE, G.S., DILEK, Y., ADAMIA, SH., OBERHÄNSLI, R.E., KARPENKO, S.F., BAZYLEV, B.A. & SOLOV'eva, N. 2007. Geochemistry and geochronology of the Neoproterozoic Pan-African Transcaucasian Massif (Republic of Georgia) and implications for island arc evolution of the late Precambrian Arabian–Nubian Shield. *Gondwana Research* **11**, 92–108.
- ZINDLER, A. & HART, S. 1986. Chemical Geodynamics. *Annual Review of Earth and Planetary Sciences* **14**, 493–571.